BRANZ

Study Report

SR343 (2016)

Numerical simulation of ventilation in roof cavities

Stephan Rupp and Manfred Plagmann

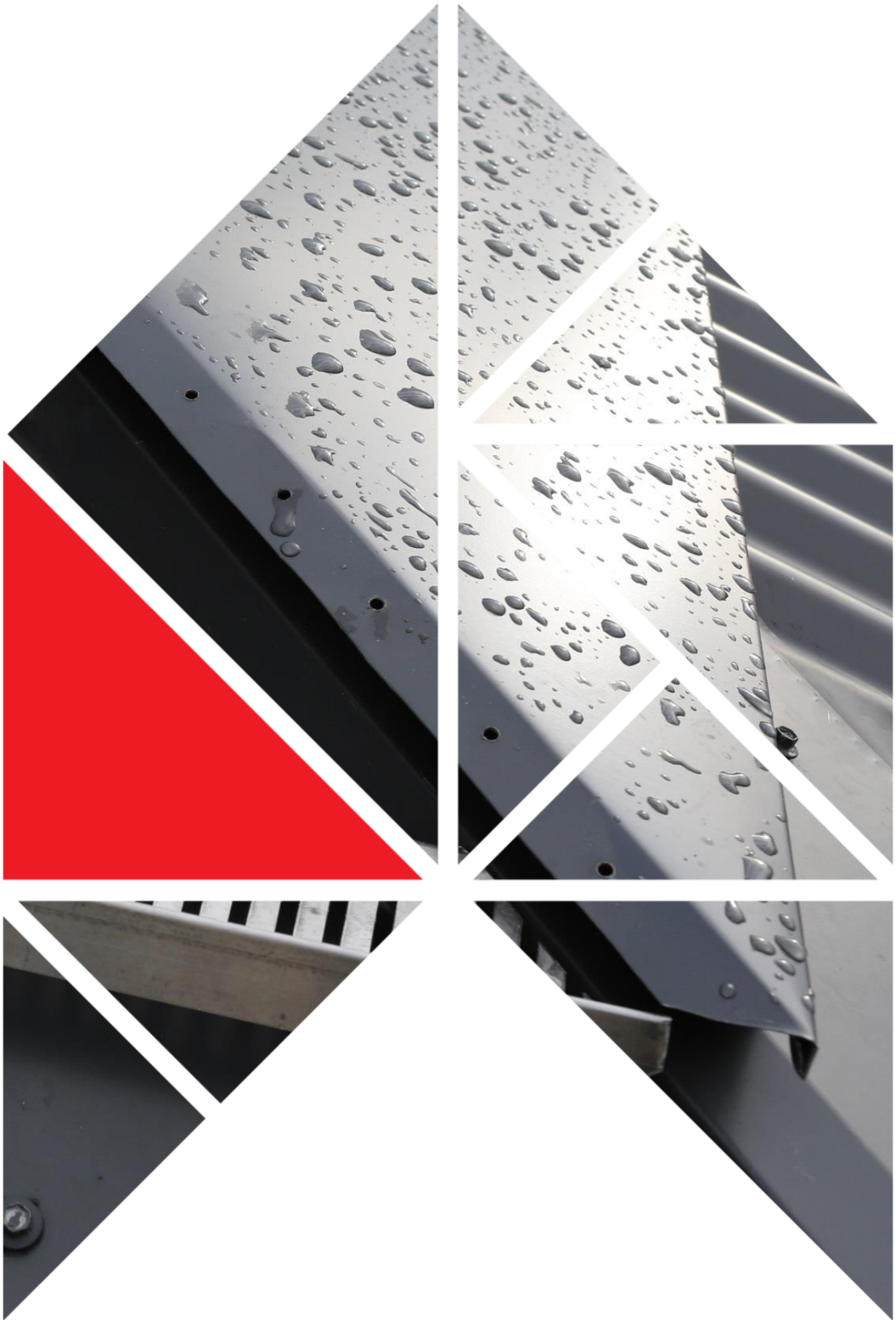

1222 Moonshine Rd
RD1, Porirua 5381
Private Bag 50 908
Porirua 5240
New Zealand
branz.nz

Funded from the Building Research Levy

MINISTRY OF BUSINESS, INNOVATION & EMPLOYMENT
HĪKINA WHAKATUTUKI

The work reported here was jointly funded by BRANZ from the Building Research Levy, the Ministry of Business, Innovation and Employment.

© BRANZ 2016
ISSN: 1179-6197

Preface

This study report covers some aspects of the Interstitial Moisture stream of the Weathertightness, Air quality and Ventilation Engineering (WAVE) project conducted at BRANZ from 2009 to 2015. Further work conducted within this stream is referenced in the report.

Acknowledgements

This work was jointly funded by the Building Research Levy and the Ministry of Business, Innovation & Employment. The insightful discussion with groups and bodies throughout the industry sector are acknowledged.

Numerical simulation of ventilation in roof cavities

BRANZ Study Report SR343

Author(s)

Stephan Rupp and Manfred Plagmann

Abstract

A numerical simulation tool is used to study the effects of installing additional ventilation channels to the roof cavities of typical New Zealand residential buildings. The simulation software was written specifically for this purpose and is based on a nodal model approach, where the building components are represented as nodal points with set properties, interacting with each other. A standard gable-type roof as well as a skillion-type roof are used for the simulations. These two roof types are placed in four different geographical climate zones: Auckland, Taupo/Turangi, Wellington and Central Otago. In addition, we investigate the properties of an ideally ventilated roof cavity. Results for the summer and winter months and a range of wind speed conditions are given. The findings are presented in terms of the probability of condensation conditions developing in the roof cavities. While absolute probabilities are stated in the report, they are mainly to be taken for comparative purposes. Additional ventilation channels are found to reduce the overall number of condensation events for both roof types in comparison to a roof without vents. In some cases, the length of a condensation event was also reduced. The skillion roof is found to be more susceptible to higher condensation event probabilities than the gable roof. It is demonstrated that reducing the moisture load in the living spaces by adequate ventilation downstairs can significantly reduce the condensation probabilities in the roof space upstairs.

Keywords

Roof Ventilation, Cold Roof, Roof Moisture.

Contents

1. INTRODUCTION 1
1.1 Scope 1
1.2 Background 1
2. EXPERIMENTAL 3
2.1 Residential gable roof building 3
2.1.1 Airflow characterisation using tracer gases 4
2.1.2 Airflow characterisation using CONTAM 10
2.2 Residential skillion-type roof 13
2.2.1 Airflow characterisation 14
3. NUMERICAL SIMULATION 18
3.1 Climate data and geographical locations 18
3.2 Nodal modelling 20
3.2.1 What is a nodal model? 20
3.2.2 Nodal model mathematics 21
3.3 Materials and resistances 22
3.4 Input parameters 23
3.5 Sky radiation model 23
3.6 Undercooling 23
3.7 Model description – open steel roof 24
3.8 Model description – gable Roof 26
3.9 Model description – skillion roof 29
4. RESULTS 32
4.1 Baseline model – open steel roof 32
4.2 Gable roof 33
4.3 Skillion roof 39
5. CONCLUSION 44
REFERENCES 45

Figures

Figure 1. Residential building with standard gable roof construction used for airflow resistance measurements. The entrance side of the house shown here is oriented towards the north. 3
Figure 2. Ridge cap and soffit vents installed at the National Park building. 4
Figure 3. Measured Freon and SF_6 concentrations in the roof cavity and living room (vents sealed). 5
Figure 4. Temperature, relative humidity and wind speed measurements during the vents-sealed experiment. 6
Figure 5. Infiltration and exfiltration rates for the National Park gable roof building (roof cavity vents sealed). The high initial values are an artefact. 7
Figure 6. Wind speed as recorded during the vents open experiment. 8
Figure 7. Infiltration and exfiltration rates for the National Park gable roof building (roof cavity vents open) 9

Figure 8. Representation of the National Park building as a CONTAM airflow model. The circles represent airflow channels such as natural openings in walls and roofs as well as artificial vent openings (eaves and ridge vents). Green and red bars represent airflow and pressure differences respectively across an airflow resistance and a given wind speed and direction.....10
Figure 9. Pressure coefficients Cp for the north-facing wall, as a function of wind direction.....11
Figure 10. Comparison of measured (dots) and simulated (lines) Freon (left) and SF_6 (right) gas concentrations for the sealed vents case and for the two zones – living room and roof cavity. The simulated SF_6 concentration in the living room is close to zero and largely obscured by the measured data points. 12
Figure 11. Comparison of measured (dots) and simulated (lines) Freon (left) and SF_6 (right) gas concentrations for the open vents case and for the two zones – living room and roof cavity. 13
Figure 12. Skillion-type roof with some of the ceiling panels removed (left). Ventilation channels were added at the northern and southern eaves (right).....14
Figure 13. Representation of the skillion roof test set-up with its three zones (outside, roof cavity and living space) and the airflow resistances (R2 – ceiling, R3 –walls and R1 – roof including vent elements) between the zones. It is necessary to isolate and characterise each individual resistance element. The photo on the left shows the fan mounted to pressurise the lower container volume. 14
Figure 14. Left: two-fan set-up to characterise the roof cavity to ambient airflow resistance only, avoiding any back flow into the container space. Right: single-fan set-up to measure the roof cavity properties including the ceiling. 15
Figure 15. Experimental characterisation of the roof cladding airflow resistance, following the two-fan approach described in the text. The pressure difference is measured between the roof cavity and ambient.....15
Figure 16. Measured (dots) and CONTAM simulation (line) of the Freon and SF6 gas concentrations in both zones of the skillion roof test set-up. Blue graphs refer to the roof cavity zone, while brown refers to the lower living space zone. The eaves vents were sealed in this case.....17
Figure 17. Measured (dots) and CONTAM-simulated (lines) gas concentrations for the vents open case.....17
Figure 18. Winter and summer temperature statistics for the four climate zones. Displayed are maximum, 75% quantile, median, 25% quantile and minimum temperatures. Data by NIWA. 18
Figure 19. Nodes in building components describe the building as a physical system..20
Figure 20. Section of the graphical representation of a nodal model with an edge property overlay. 21
Figure 21. Cooling potential below ambient temperatures at various locations during the summer (S) and winter (W) months.....24
Figure 22: Open steel roof model outline of nodes and their interconnections. 25
Figure 23. Sketch of the gable and skillion roof nodes and their interconnections.....29
Figure 24. Idealisation of a warm roof and a completely ventilated roof cavity.....32
Figure 25. Condensation statistics for the gable roof in the Taupo/Turangi zone for the winter months and the three wind speeds: comparison between open and closed vents. 35
Figure 26. Condensation statistics for the gable roof in the Taupo/Turangi zone for the summer months and the three wind speeds: comparison between open and closed vents. 35

Figure 27. Condensation statistics for the gable roof in the Auckland zone for the winter months and the three wind speeds: comparison between open and closed vents. 36
Figure 28. Condensation statistics for the gable roof in the Auckland zone for the summer months and the three wind speeds: comparison between open and closed vents. 36
Figure 29. Condensation statistics for the gable roof in the Wellington zone for the winter months and the three wind speeds: comparison between open and closed vents. 37
Figure 30. Condensation statistics for the gable roof in the Wellington zone for the summer months and the three wind speeds: comparison between open and closed vents. 37
Figure 31. Condensation statistics for the gable roof in the Central Otago zone for the winter months and the three wind speeds: comparison between open and closed vents 38
Figure 32. Condensation statistics for the gable roof in the Central Otago zone for the summer months and the three wind speeds: comparison between open and closed vents. 38
Figure 33. Indoor relative humidity during the winter period with an indoor air infiltration of about 0.5 ACH. 39
Figure 34. Condensation probability in the roof cavity depending on roof ventilation and geographic location during winter. 39
Figure 35. Example from Central Otago showing the dependence of the roof condensation probability on the indoor-outdoor room air exchange rate. The red dot is at about 0.55 ACH, which is within range of the air exchange rate recommended by the World Health Organisation. This exchange rate is then used in all subsequent simulations. 40
Figure 36. Impact of roof ventilation on the condensation probability. The results are based on a room ventilation of about 0.5 ACH. 41
Figure 37. Condensation hour distribution for Auckland at roof air exchange rates between 14 to 66 ACH 41
Figure 38. Condensation hour distribution for Taupo/Turangi at roof air exchange rates between 14 to 66 ACH 42
Figure 39. Condensation hour distribution for Wellington at roof air exchange rates between 14 to 66 ACH 42
Figure 40. Condensation hour distribution for Central Otago at roof air exchange rates between 14 to 66 ACH 43

Tables

Table 1. Approximate ventilation rates and ventilation ratios for the gable roof building for light wind conditions. 9
Table 2: Airflow channels and their physical properties used in the CONTAM model for the National Park building. 12
Table 3. Airflow resistances for the skillion roof test container. 16
Table 4. Wind speed statistics for the four climate zones used in this study. Given are the wind speeds in (m/s). A value of 6.1 m/s in the 75% quantile bracket means that 25% of the recorded speeds are greater than 6.1 m/s. The data by NIWA is based on hourly averages. 19

Table 5. Wind parameters as an input to the CONTAM building airflow calculation. 19
Table 6. Symbols used in the nodal model equations. 21
Table 7. General materials properties used in the nodal model simulations. 23
Table 8. Input parameters to the nodal model simulations. 23
Table 9. Properties of the open steel roof nodes. 24
Table 10. Interconnection properties between the nodes in the open steel roof nodal model. 25
Table 11. Dimensions of the gable roof building at National Park. 26
Table 12. Nodes for the gable roof model. 27
Table 13. Nodal interconnection properties. 28
Table 14. Dimensions of the skillion roof test container. 29
Table 15. Nodes for the skillion roof model. 30
Table 16. Interconnections between the skillion roof nodes. 31
Table 17. Percentage of time the underside of roofing cladding of an ideally ventilated roof cavity will be in a condensation or wetness condition. 33
Table 18. Percentage of time the gable roof cavity will be in a condensation condition. Closed and open vents configurations are given. 34
Table 19. Percentage of time the skillion roof cladding will be under condensation condition depending on the outdoor-roof air exchange rate. 43

1. Introduction

1.1 Scope

This study report covers some aspects of the Interstitial Moisture stream of the Weathertightness, Air quality and Ventilation Engineering (WAVE) project conducted at BRANZ from 2009 to 2015. In particular, this report investigates the implications of adding additional ventilation channels between the ambient and a roof cavity. Previous work within this WAVE stream has been published elsewhere and includes Study Report SR289 *Remediating condensation problems in large-cavity, steel-framed institutional roofs* (Cunningham and Quaglia, 2013) and a technical discussion document – *Initial guidance on the moisture design of large-span roofs for schools* (BRANZ, 2015). Following on from these publications, we now endeavour to use a more generic approach using numerical simulation to determine if and how additional ventilation can be used to decrease the moisture levels in roof cavities. The performance of a building and its roof cavity depends on a great number of parameters, including occupancy behaviour. While it is not possible to cover the whole parameter space, we tried to cover what seems most relevant for New Zealand conditions. To conduct the numerical calculations, we have chosen to write our own software routine based on a nodal approach, which offers some benefits over existing software packages. This report describes our nodal model in some detail. Only cold roof designs are considered here.

1.2 Background

Residential and commercial building techniques have changed significantly over the last decades in New Zealand. In particular, the building envelope airtightness and thermal insulation levels have increased, mostly to achieve higher indoor temperatures or reduced heating costs. While buildings in the past had an intrinsically high level of natural ventilation, this is not true anymore for a growing number of buildings built after 1990. These trends can have unexpected ramifications on the performance of other parts of the building. For instance, an increased level of thermal insulation in the ceiling will decrease the winter temperature in the roof cavity above. The climatic conditions in New Zealand, with its high relative humidity, may have the potential to cause problems. An increased number of reports of excessive condensation within roof cavities does seem to be related to changing building techniques as they are often encountered in newly built houses. The complexity should not be underestimated as there are numerous factors that can cause a design to fail, and ventilation might not be able to compensate for other flaws.

The time-dependent moisture balance of a building or part of the building such as the roof cavity is governed by the sources of moisture, moisture removal and moisture storage. Sources of moisture can be internal – respiration and perspiration, clothes drying, bathroom activities, cooking, unflued gas heating and so on (Elkink, 2012) – and external. The internal sources depend significantly on the number of occupants as well as their behaviour patterns. Education of occupants on the proper usage of a building has become more relevant as houses have become more sealed. External sources of moisture are generally humid air[1] that is brought into the building from the

[1] Moisture from rain penetration through leaks in the building envelope are not considered in this study.

outside or the subfloor area via infiltration[2] or artificial ventilation channels. The moisture content of the outside air is of course a function of geographical location and weather conditions. It can be essentially zero in cold, continental climates to a maximum of about 0.02 kg_{Water} / kg_{DryAir} in humid climates. In New Zealand, values are of the order of 0.005 kg_{Water} / kg_{DryAir}.

Moisture removal mechanisms include ventilation (if the inside moisture content is higher than the air it is replaced with)[3] and internal moisture removal such as dehumidifiers. (Desiccants are commercially available but only for small enclosures.) Only the effects of ventilation are considered in this study. Moisture can be stored in furnishings, timber and other building materials. For the roof cavity, only the moisture storage in the construction timber is relevant.

It is worthwhile pointing out that adding artificial ventilation channels to the roof cavity cannot guarantee a climate free of condensation events. Even an ideally ventilated cavity will contain air that has the same moisture content as the surrounding atmosphere. The roof surface can drop to temperatures well below the ambient during clear nights, reaching the dew point temperature and leading to condensation. Ventilation can only help if the moisture level is raised above the ambient by sources within or from below the roof cavity.

Consequently, removing excess moisture from a roof cavity by additional passive or active ventilation channels should be the last step, as vents may have detrimental effects such as increased heat loss or increased corrosion. To reduce the need for roof cavity ventilation, these measures should be considered first:

- Minimise moisture generation within the building (avoid drying clothes inside, unflued gas heaters and so on).
- Remove excess moisture by ventilation of living spaces. Heat exchangers are an option to minimise heat loss.
- Minimise moisture transfer from the living space into the roof cavity by minimising air leakage paths into the roof space (for example, replace old, open downlights with tight-fitting LED lights, replace leaky hatches and seal gaps).

To illustrate this point, we have looked at a baseline case where an existing roof cavity is ideally ventilated, i.e. it always has air of ambient condition without any additional moisture sources. It is assumed that the ceiling is absolutely tight, both in terms of air and heat exchange from the living quarters below to the roof cavity above.

[2] Infiltration channels are defined as unintentional openings in the building envelope, such as gaps around windows that cannot be readily shut. Ventilation channels are purposefully engineered openings.

[3] Absolute moisture content is sometimes a more useful measure than relative humidity (RH). For instance, a parcel of outside air at 30°C and 40% RH has a higher moisture content than air-conditioned inside air of 20°C and 50% RH.

2. Experimental

In order to simulate the heat and moisture transfer properties of a building, we need some information of the airflow resistances of each individual boundary of the building. This parameter describes the relationship between the pressure difference in pascals [Pa] and the airflow [m^3/s] across a boundary. Pressure differences driving air exchanges are usually caused by wind across the building envelope or temperature differences (stack effect). The process of isolating and characterising these airflow resistances is described in this section.

Two buildings are used as the experimental basis for the simulation work in this study. First, we have installed a skillion-type roof on our roof-test container, which was described earlier in Cunningham and Quaglia (2013).

2.1 Residential gable roof building

In order to simulate a residential building with a standard truss roof construction, we have characterised the airflow resistances of a two-bedroom building at National Park in the Taupo/Turangi climate zone (Figure 1). This particular building was chosen, as artificial vent openings were added to the roof cavity after the original roof design had developed condensation problems. We were able to temporarily seal off these openings, thus gathering and comparing data for a vented and unvented gable roof cavity in a real-life situation.

Figure 1. Residential building with standard gable roof construction used for airflow resistance measurements. The entrance side of the house shown here is oriented towards the north.

The single-level building was erected on a level section within a semi-urban environment. The living space floor area is approximately 59 m^2 (volume 140 m^3), while the roof cavity encloses a volume of about 44 m^3. The building is erected on wooden piles with a well ventilated subfloor space. The two bedrooms are located on the eastern side of the building, and the western end has a bathroom and a drying room/laundry. The kitchen and living areas are combined in the central part of the house.

The building was originally erected without additional vent openings in the roof cavity. Problems were noticed especially during cold nights and a high internal moisture load (up to eight occupants, wet clothing and so on) when condensation and ice were forming in the roof cavity. The owner then decided to install soffit and ridge cap vents to increase the air exchange in the roof cavity (Figure 2).

Figure 2. Ridge cap and soffit vents installed at the National Park building.

The custom-made ridge cap ventilation extends along all four sides of the ridge with a combined length of 12.4 m. The net opening of the vent is around 15,300 mm^2/m, yielding a total area of approximately 190,000 mm^2. The round soffit vents are installed on all four sides of the building with fewer on the western side. Each individual vent contributes 2500 mm^2 of net opening. There are 91 elements installed, giving a total soffit vent opening size of 227,500 mm^2. The net total ventilation opening is often put in relation to the total attic floor space (Iffa and Tariku, 2015). In this case, this ratio is ($0.43m^2/59m^2$), approximately 1/140, which is slightly higher than what other building codes recommend. Depending on climate zones, ratios between 1/150 and 1/300 are often mentioned (Iffa and Tariku, 2015). However as Rose (1992) points out, the standard rule of thumb for ventilation in attic assemblies of 1/300 is based on some rather incomplete experimental work. The combination and location of soffit and ridge vents have been studied by Iffa and Tariku (2015). In wind-driven situations, locating the upper vent close to the ridge line (as in our situation) will result in a slightly lower air exchange rate but will minimise volumes that are not affected by the air exchange.

2.1.1 Airflow characterisation using tracer gases

In order to understand air, heat and moisture transport throughout the building, the airflow resistances for key building elements such as walls, ceilings and roofs need to be determined. An airflow resistance expresses the relationship between pressure differences across an opening and the resulting airflow across it. The relationship can be expressed as

$$Q = C\,|\,\Delta P|^{n} \qquad \text{[Eq1]}$$

where Q is the airflow rate in [m^3/h], ΔP is the pressure difference in [Pa], C is the characteristic coefficient and n is the characteristic exponent. Pressure differences across walls, ceilings and roofs are usually caused by temperature differences (stack pressure), wind action or active elements such as ventilation fans. Blower door measurements are one way to determine the characteristic coefficient C and n. However, in order to characterise single elements like the ceiling, all other elements (walls, floors, windows and so on) have to be sealed off completely. Details on how this can be achieved are given in section 2.2. For the gable roof building, we have

chosen to use a different method. Tracer gas measurements have long been used to characterise ventilation rates in buildings. This technique has been reviewed by Sherman (1990). Essentially, in our case, characteristic tracer gases are released at a constant rate into both cavities – the living quarters and the roof cavity. Freon was used for the living quarters and SF_6 for the roof cavity. By monitoring gas concentrations in both zones over time, conclusion can be drawn on the air exchange between each zone and the ambient as well as an exchange between the two zones themselves.

The airflow resistance experiments were conducted over 3 days in November 2014. First, all purpose-built ventilation channels were sealed as best as possible. The plastic eaves vents were sealed with self-adhesive tape, the ridge vent was sealed from inside the roof cavity by mounting timber boards (with compressible foam tape around the perimeter) across the openings. Freon gas was then released at a rate of 15 ml/min into the living room, while SF_6 was set to a dosing rate of 20 ml/min into the roof cavity. Several dosing tubes were located throughout the building to achieve a homogeneous gas distribution. Sampling tubes were also distributed at various points. In addition, a fan was used downstairs to aid the mixing. An initial burst of the two gases took the tracer gas concentration to some measurable level.

The gas concentrations were then measured over time using an INNOVA 1412[4] photoacoustic gas monitoring instrument. Freon and SF_6 concentration levels were sampled every 5 minutes in the living room and the roof cavity, resulting in four measured tracer gas concentrations per scan (Figure 3).

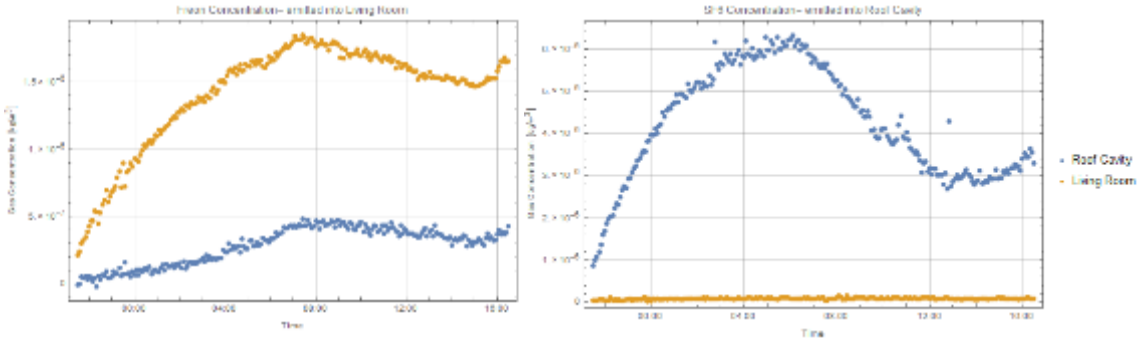

Figure 3. Measured Freon and SF_6 concentrations in the roof cavity and living room (vents sealed).

Wind direction and wind speed were also recorded during the experiment, using a mobile weather station installed some distance away from the building.[5] This allowed us to correlate the inside gas concentrations to external driving forces. Temperature and relative humidity (RH) were recorded in the roof cavity and inside the living room as well as outside using thermocouples and capacitive sensors respectively (see Figure 4). The inside temperature was maintained by a central heating system at close to 18°C.

The measurements were conducted while the building was unoccupied, so no moisture sources from occupants, cooking, bathroom, dryer and so on were present. The outside relative humidity was consistently high, above 90% for most of the time.

[4] LumaSense Technologies (www.lumasenseinc.com)
[5] The speed resolution of the anemometer was low with steps of 0.4 m/s.

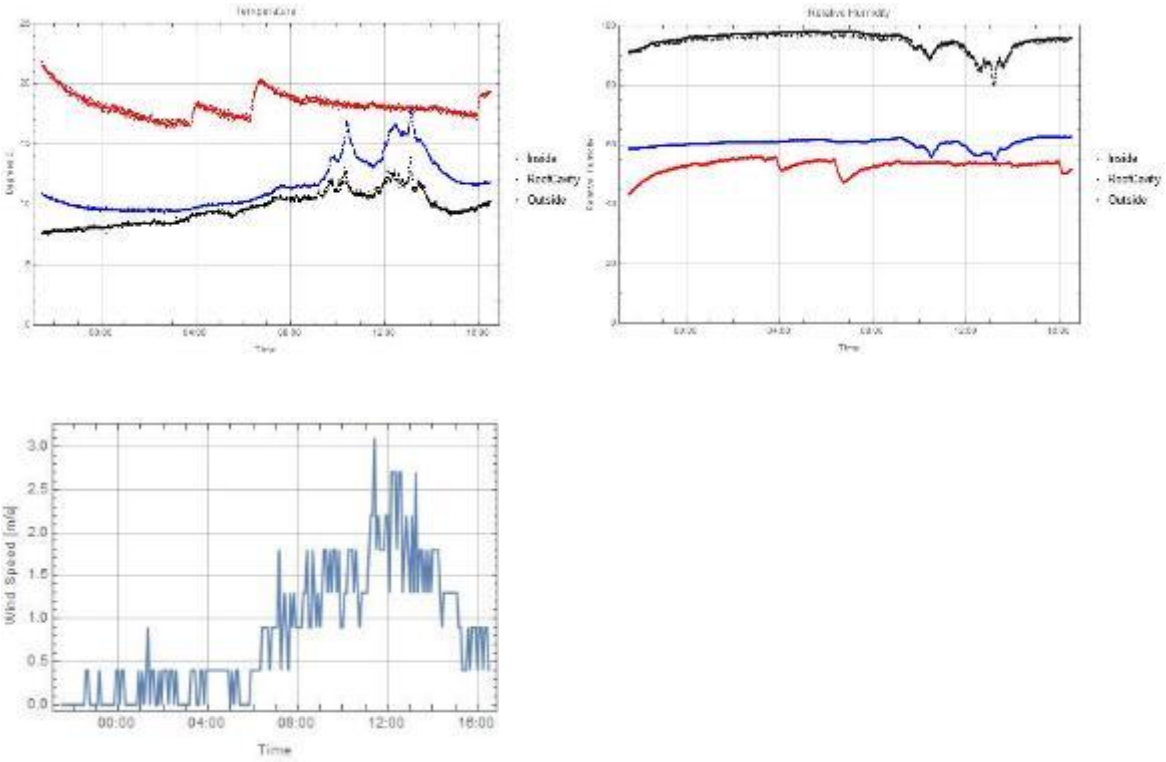

Figure 4. Temperature, relative humidity and wind speed measurements during the vents-sealed experiment.

The rapid interaction between the ambient and the roof cavity climate, even in the sealed case, is evident in Figure 4. As the wind picked up in the morning, a warmer, drier outside air mass enters the roof cavity without significant delays. The effect of warmer, drier outside air is not visible on the inside due to the heating system.

Using the measured gas concentrations versus time, the instantaneous air exchange rates between the two separate zones for the building (downstairs living area and the roof cavity) and the ambient can be calculated (Sherman, 1990). This calculation is based on assumptions that, in reality, are never perfectively achieved.

One such assumption is that the gases are perfectly mixed and homogeneous. For instance, any outside air entering the building is assumed to be instantaneously dispersed within the zone. In reality, there will be a finite time for this to happen. As described above, measures have been taken to aid the mixing of the gases and to obtain representative samples from throughout the zones.

The infiltration and exfiltration rates calculated from the measured gas concentrations of the sealed case are displayed in Figure 5. The high initial values up to midnight of the first day are probably an artefact due to the fact that the gas concentrations have not reached an equilibrium yet. Solving the set of linear equations will yield airflows across the ceiling in both directions (Q_{12} and Q_{21} in Figure 5). However, as expected, one of these flow values is close to zero, while the other, Q_{12}, has consistent positive values.

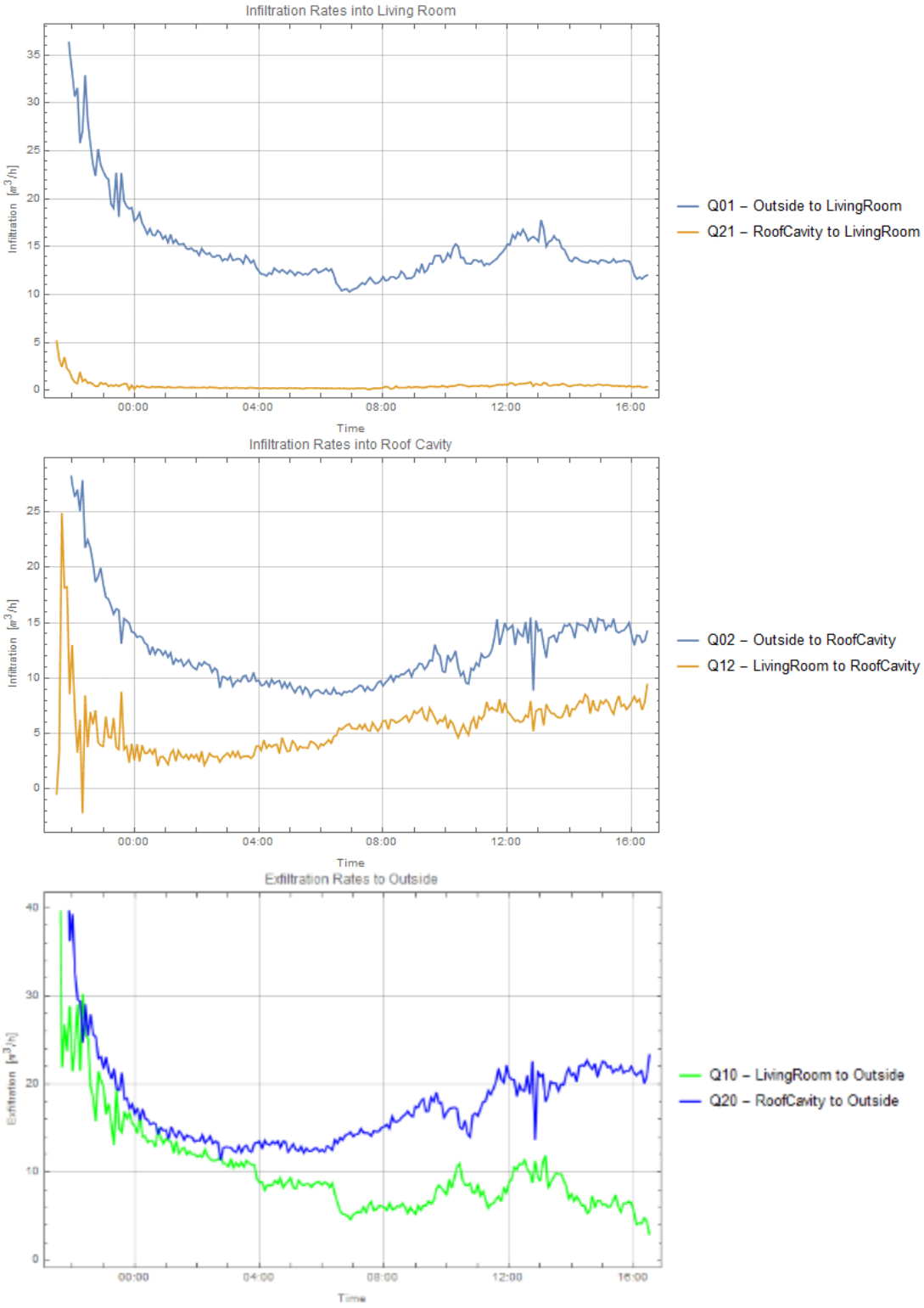

Figure 5. Infiltration and exfiltration rates for the National Park gable roof building (roof cavity vents sealed). The high initial values are an artefact.

The second part of the investigation was to open the roof cavity ventilation channels and repeat the tracer gas experiment. In anticipation of an increased air exchange in the roof cavity, we increased the SF_6 dosing rate to 30 ml/min while retaining 15 ml/min for the Freon gas in the living room zone. The climatic conditions were similar to the vents-sealed experiment, with the peak wind speed slightly lower (Figure 6).

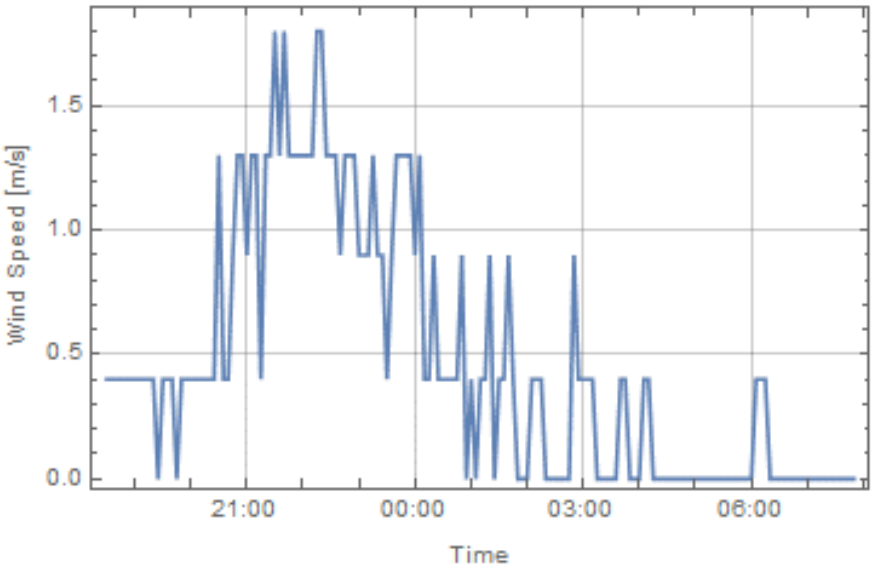

Figure 6. Wind speed as recorded during the vents open experiment.

Calculating again the infiltration and exfiltration rates from our time-dependent gas concentration measurements in the two zones, we find a significantly changed situation (Figure 7) for the vents open case. While the air exchange between the ambient and the living room zone is of the same order of magnitude as in the vents-sealed case, the roof cavity air exchange has vastly increased.

During the hours of higher wind speed between 21:00 and 00:00, we find infiltration/exfiltration rates of the roof cavity to the ambient between 100 and 200 m^3/h. This is an order of magnitude higher than in the sealed case. The flow from the living room zone to the roof cavity is also increased during the peak wind hours to values around 25 m^3/h.

Ventilation rates are commonly described by air changes per hour [ACH] for a given building zone volume. It is evident from the figures in this section that values for air exchange will be a function of wind speed and direction. Thus, robust and meaningful statements will have to be derived using statistical climate data. It is nevertheless useful to calculate the ventilation rates for a normal wind condition.

Table 1 lists the approximate ventilation rates for the living room and the roof cavity. The low ventilation rates are due to the fact that the wind speed was very low during the experiments. The effect of opening the roof cavity vents is clearly visible by an increase in the ventilation rate by a factor of approximately 3.

The table also gives an approximate ventilation ration of the roof cavity. This parameter is defined as $Q_{02} / (Q_{02} + Q_{12})$, where Q_{02} is the ambient-to-roof cavity flow and Q_{12} the living room-to-roof cavity flow. A value of 1 would indicate that there is no upwards transport of (possibly moist) living room air into the roof cavity and that the latter is ventilated only with fresh ambient air.

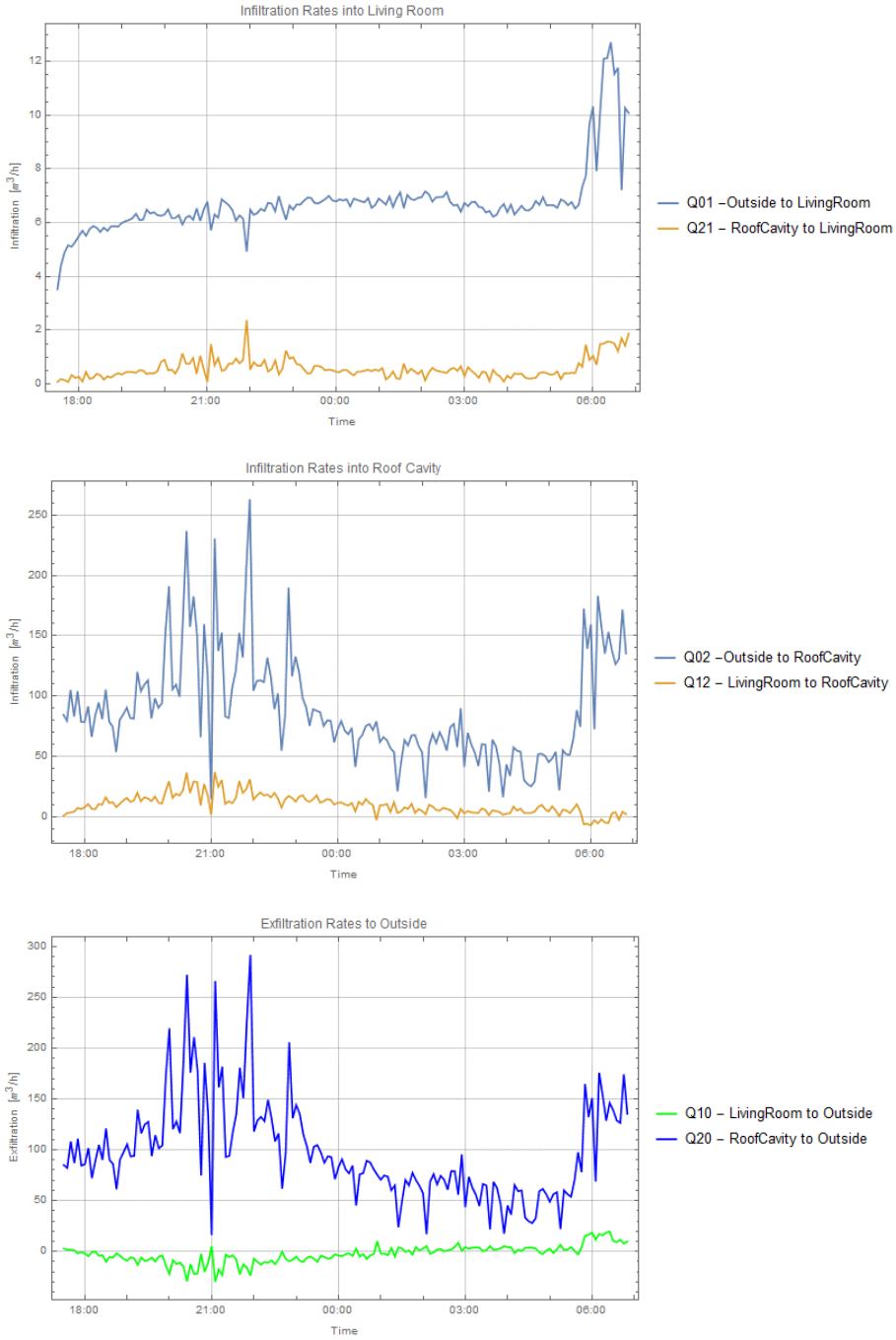

Figure 7. Infiltration and exfiltration rates for the National Park gable roof building (roof cavity vents open).

Table 1. Approximate ventilation rates and ventilation ratios for the gable roof building for light wind conditions.

Roof Cavity Vent Elements	Zone	Volume [m^3]	Wind speed [m/s]	approximate Ventilation rate [ach]	Ventilation Ratio [-]
Sealed	Living Room	140	0.75	**0.1**	
	Roof Cavity	45	0.75	**0.5**	**0.63**
Open	Living Room	140	0.75	**0.1**	
	Roof Cavity	45	0.75	**1.8**	**0.88**
			1.8	**5.5**	**0.89**

2.1.2 Airflow characterisation using CONTAM

The data obtained from the tracer gas experiments is now used to create a numerical airflow model of the building. Such a model enables us to simulate the airflows throughout the building for any desired wind speed, wind direction and temperature distribution. Knowledge of the airflow patterns of a building over time is a key parameter in understanding moisture transport. The fact that airflow is dominating over diffusion when it comes to moisture transport has been widely published [7].

We used the freely available numerical simulation software CONTAM [8] created by the US National Institute for Standards and Technology (NIST), for our building models. CONTAM has been created specifically for this purpose, capable of simulating wind, buoyancy and mechanically driven airflows in multizone buildings.

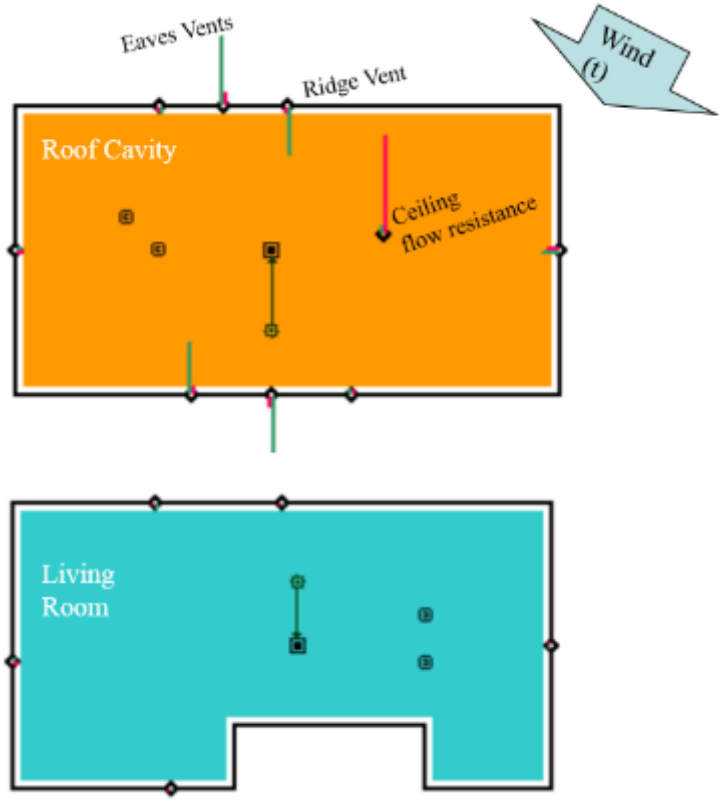

Figure 8. Representation of the National Park building as a CONTAM airflow model. The circles represent airflow channels such as natural openings in walls and roofs as well as artificial vent openings (eaves and ridge vents). Green and red bars represent airflow and pressure differences respectively across an airflow resistance and a given wind speed and direction.

The National Park building is translated into a two-zone CONTAM model by combining the living quarters into a downstairs zone with the roof cavity constituting the second zone. Building footprint, volumes and geographical orientation are entered into the model, but any internal walls are disregarded. As described above, the temperature and humidity within each zone is assumed homogeneous.

The airflow resistances in the CONTAM model are either defined according to Equation [Eq1] in terms of their coefficients C and exponent n or where the geometry is known (as in case for the eaves and ridge vent) in terms of an orifice area opening.

We have used airflow paths for each of the four outside walls in the living room zone, one opening on the southern side (trickle vent window) and one airflow resistance from the living room to the roof cavity (ceiling flow resistance). The roof cavity zone has the four eaves vent channels characterised by their geometry as well as the ridge vent. The latter was divided into two, as one side is facing north while the other is located on the southern side of the ridge. In addition, we have incorporated two general airflow channels representing a leaky north and south facing roof deck. The coefficients of these airflow resistances were then adjusted to yield good agreement of the modelled airflows and gas concentrations with the measured flows and concentrations.

In order to simulate the airflows throughout the building over time, however, we also require knowledge of the pressure distribution around the building as a result of different wind velocities and directions. Specifically, we need to estimate the pressure coefficient C_p for the locations of the airflow channels around the building envelope. This coefficient C_p is defined as

$$Cp(x,y,z) = \frac{\mathrm{p(x,y,z)} - p(\infty)}{\frac{1}{2}\rho\, v^2(\infty)} \qquad \text{[Eq2]}$$

where $\mathrm{p(x,y,z)}$ is the pressure at the desired location, $p(\infty)$ is the static pressure some distance away from the site and the denominator representing the dynamic pressure of the on-flowing air mass some distance away and thus unperturbed by the building. A Cp of 1 (the maximum it can attain) means that the complete dynamic pressure is bundled at this stagnation point. It is not possible to measure precise values of Cp for the buildings we have investigated, which is why we had to rely on some estimates. These estimates are derived from experimental work at the Tokyo Polytechnic University[6]. Here, four model-sized residential houses with slightly different gable roof designs were equipped with a large number of pressure transducers and examined in a wind channel set-up. Cp values are then derived for all of these pressure sensor locations. While the investigated buildings are not perfectly identical to our National Park building with its four sloped roof faces, the obtained Cp values will nevertheless describe the overall tendency correctly. Figure 9 gives an example of the pressure coefficients for the north wall of the building as a function of the incident wind direction.

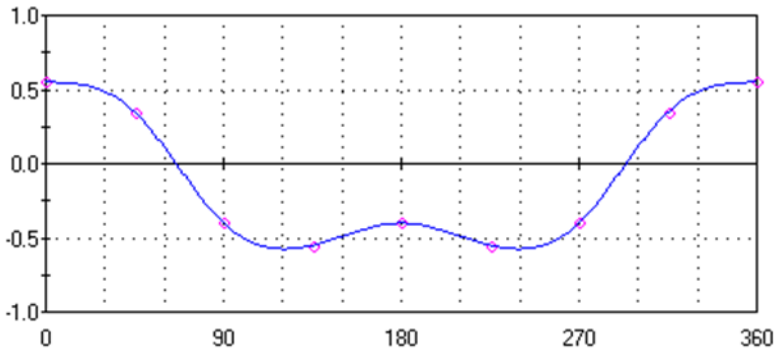

Figure 9. Pressure coefficients Cp for the north-facing wall, as a function of wind direction.

[6] www.wind.arch.t-kougei.ac.jp/info_center/windpressure/lowriseeave/mainpage.html

Table 2 summarises the airflow resistances as used in the National Park CONTAM model. As mentioned above, the coefficients *C* and exponent *n* for the individual airflow channels of this building can only be estimates. The precise distribution around the building as well as the magnitude will differ from these given values in reality.

Table 2: Airflow channels and their physical properties used in the CONTAM model for the National Park building.

Airflow channel – residential gable roof building	C [$m^3/s/Pa$]	n [1]	Opening area [m^2]	Number of elements	Used in vented case model only
North wall	0.0070	0.5		1	
East wall	0.0070	0.5		1	
South wall	0.0070	0.5		1	
West wall	0.0070	0.5		1	
South wall window opening			0.0400	1	
Ceiling	0.0010	0.5		1	
Roof north-facing	0.0300	0.5		1	
Roof south-facing	0.0300	0.5		1	
Ridge vent north			0.0950	1	Yes
Ridge vent south			0.0950	1	Yes
Eaves vents north			0.0025	41	Yes
Eaves vents east			0.0025	9	Yes
Eaves vents south			0.0025	3	Yes
Eaves vents west			0.0025	38	Yes

Further inputs to the model are the measured outdoor, living room and roof cavity temperatures as well as the measured wind direction and wind speed. As an output, CONTAM will yield the airflows as a function of time of each individual airflow resistance. In addition, CONTAM can simulate tracer gas concentrations versus time that are released at a constant dosing rate, as in our case.

The outputs of the CONTAM model – gas concentrations and airflows versus time – can now be compared to our actual measured (gas concentration – Figure 3) and derived (airflows – Figure 5) values, giving us confidence that our estimated coefficients describing the building are in the right order of magnitude.

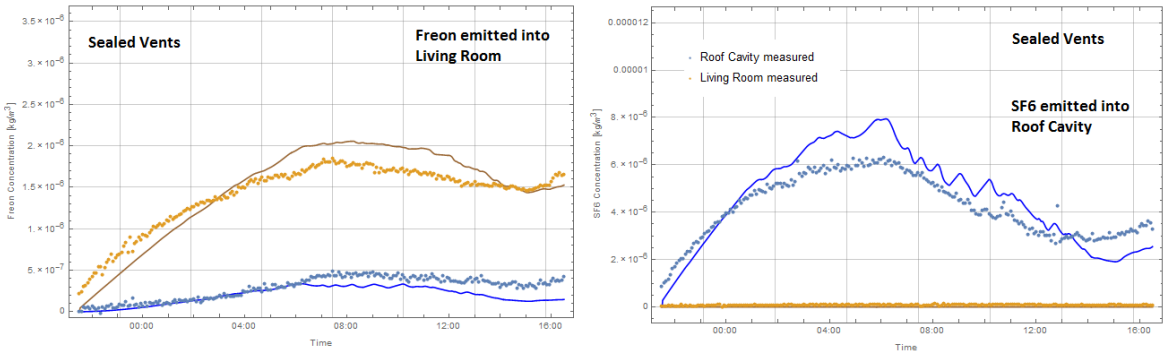

Figure 10. Comparison of measured (dots) and simulated (lines) Freon (left) and SF_6 (right) gas concentrations for the sealed vents case and for the two zones – living room and roof cavity. The simulated SF_6 concentration in the living room is close to zero and largely obscured by the measured data points.

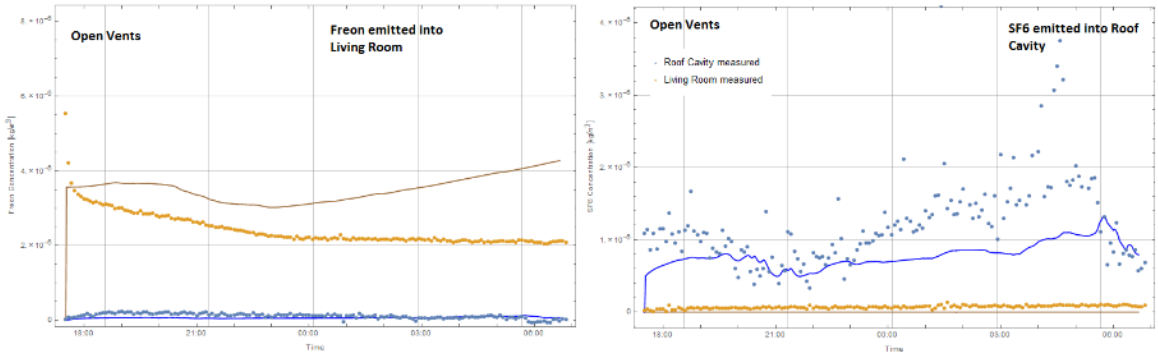

Figure 11. Comparison of measured (dots) and simulated (lines) Freon (left) and SF_6 (right) gas concentrations for the open vents case and for the two zones – living room and roof cavity.

Figure 10 and Figure 11 show the measured and simulated gas concentrations for the sealed and open vents case respectively. Each graph displays the concentration of the gas within the zone it is released to as well as the concentration in the second zone. For the sealed vents case (Figure 10) in particular, we find a very good agreement between the measured data and the CONTAM simulated gas concentration. The Freon emitted into the living room rises steadily due to the very calm wind conditions. As the wind picks up around 08:00, a plateau in the Freon concentration is reached with the concentration starting to decline towards the afternoon, indicating an increased gas exchange between the ambient and the living room zone. The Freon concentration in the roof cavity is lower by a factor of 4 but otherwise follows the same trend as in the living room. On the other hand, there is no significant level of SF_6 present in the living room, indicating that there is an upward flow only from the living room to the roof cavity for all temperature and wind conditions over the time period examined here. The agreement between measurement and simulation is less satisfactory for the open vent case (Figure 11), however still well within an order of magnitude, especially for the SF_6 gas in the roof cavity. Despite the fact that the dosing rate for SF_6 into the roof cavity had been increased for the open vent case from 20 to 30 ml/min, we see a much reduced concentration in comparison to the sealed case. This is of course in agreement with the expectation of an increased air exchange between the ambient and the roof cavity.

2.2 Residential skillion-type roof

The experiments with a skillion-type roof were conducted at our BRANZ site in Porirua utilising our roof test container, which was described previously (Cunningham and Quaglia, 2013). Figure 12 shows some pictures of the inside as well as of the ventilation channels that were added to give airflow access directly into the roof cavity in between the insulation and the roofing underlay. The six vents on either side could be opened or sealed by the plastic end caps. The footprint of the container is 2.5 m × 12 m = 30 m^2 with a total volume under the ceiling level of approximately 85 m^3. The long axis of the container is oriented in a north-south direction. The corrugated roofing iron is carried by a construction of timber purlins on timber rafters with a synthetic roofing underlay directly beneath the iron. The polyester ceiling insulation is 165 mm thick leaving a gap of 25 mm within the 190 mm wide rafters. The purlins of 45 mm thickness add further volume to the roof cavity. The free roof cavity volume above the insulation is approximately 2 m^3, so if we include the volume of the insulation, we have a total volume of 6.5 m^3. The 2 × 6 ventilation channels directly access the free roof

cavity volume. No ridge cap ventilation was installed on this low-sloping roof. Care was taken to seal the roofing iron as best as possible around the perimeter. The ceiling is standard plasterboard.

Figure 12. Skillion-type roof with some of the ceiling panels removed (left). Ventilation channels were added at the northern and southern eaves (right)

2.2.1 Airflow characterisation

The flow resistances for the elements of the skillion roof test set-up were obtained by a series of airflow and pressure measurements. Details are given in Cunningham and Quaglia (2013). Essentially, a blower door fan is used to pressurise a cavity while measuring the airflow and pressure difference across the boundary. By stepping through a number of airflow settings, a graph based on Equation [E1] can be created and fitted to obtain the characteristic parameters *C* and *n*.

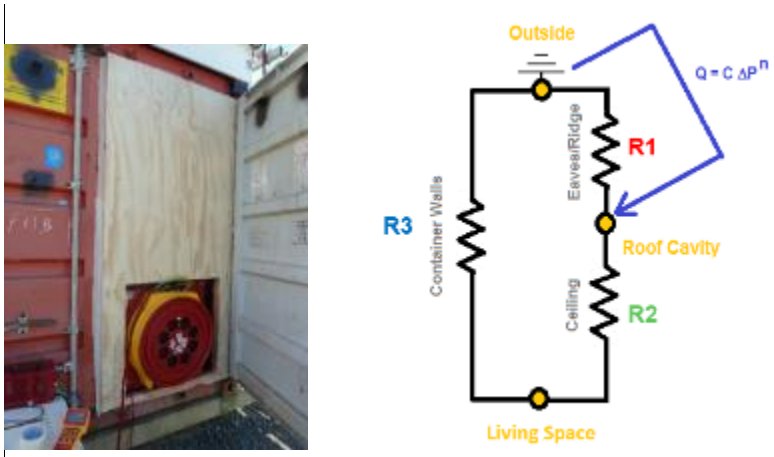

Figure 13. Representation of the skillion roof test set-up with its three zones (outside, roof cavity and living space) and the airflow resistances (R2 – ceiling, R3 – walls and R1 – roof including vent elements) between the zones. It is necessary to isolate and characterise each individual resistance element. The photo on the left shows the fan mounted to pressurise the lower container volume.

In order to characterise each individual airflow resistance (Figure 13), it is either necessary to completely seal off any other possible flow paths or to use a second fan to create a counter pressure to balance the pressure difference across the boundary to zero.

The latter method is visualised in Figure 14. The aim here is to characterise the airflow resistance R1 from the roof cavity to ambient, which includes the flow through the roof cladding and any installed vent elements. This is done by pressurising the roof cavity using Fan 1 and measuring the airflow into the cavity and the pressure difference from the cavity to ambient. To avoid any airflow from the pressurised roof cavity down into the container space across resistance R2, which would falsify our results, we used a second Fan 2 providing an adjustable airflow to balance the pressure across the ceiling to zero.

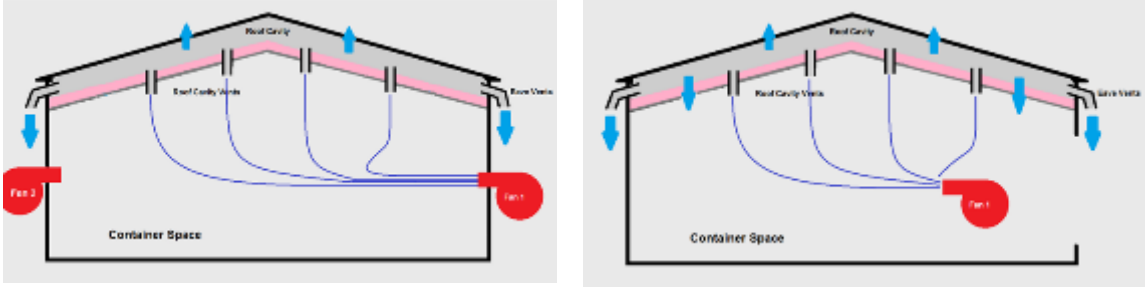

Figure 14. Left: two-fan set-up to characterise the roof cavity to ambient airflow resistance only, avoiding any back flow into the container space. Right: single-fan set-up to measure the roof cavity properties including the ceiling.

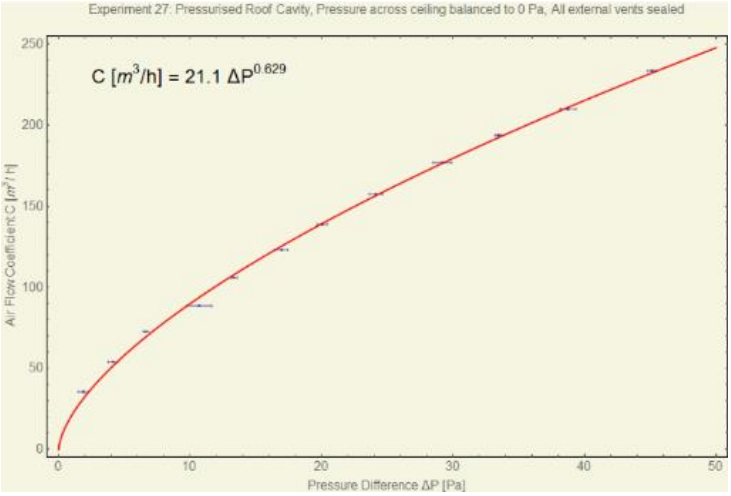

Figure 15. Experimental characterisation of the roof cladding airflow resistance, following the two-fan approach described in the text. The pressure difference is measured between the roof cavity and ambient.

Figure 15 gives an example of the experimental data that we obtained for the balanced two-fan set-up. The airflow into the cavity was measured with a calibrated laminar-flow element, which gave better results than the commercial blower door fan. With the roof cladding airflow resistance known, the ceiling resistance can be isolated by conducting an experiment, pressurising the cavity with the single-fan set-up only and the container space opened to the atmosphere.

Table 3. Airflow resistances for the skillion roof test container.

Airflow channel – skillion roof set-up	C [m3/s/Pa]	n [1]	Opening area [m²]	Number of elements	Used in vented case model only
North wall	0.00295	0.699		1	
East wall	0.00295	0.699		1	
South wall	0.00295	0.699		1	
West wall	0.00295	0.699		1	
Ceiling	0.00186	0.872		1	
Roof north-facing	0.00293	0.629		1	
Roof south-facing	0.00293	0.629		1	
Eaves vents north			0.00196	6	Yes (3 used only)
Eaves vents south			0.00196	6	Yes (3 used only)

With the skillion roof test set-up now characterised for its airflow resistances, we have conducted again tracer gas measurements to confirm the overall validity of these values. In the first experiment conducted in March 2015, the eaves vents were sealed off and Freon (7 ml/min) and SF_6 (4 ml/min) released in the lower container space and the roof cavity respectively.

To ensure that the gas is released as homogeneously as possible in the small skillion roof cavity, the dosing and sampling tubes were split into several branches reaching well into each subsection of the cavity. Care was taken to ensure that representative gas samples were obtained by calculating the total tube volume. The gas analyser was then set to flush an appropriate volume before taking each reading. The wind conditions for both the sealed and open vents experiments were unsteady both in terms of wind speed and wind direction.

Temperatures and relative humidity were measured inside the container zone, in the roof cavity as well as outside. Temperature versus time is an input to the CONTAM airflow simulation. The inside temperature oscillated between 22°C and 17°C in the lower zone while the roof cavity temperature reached values between 6°C and 45°C.

Figure 16 shows the comparison between measured and simulated gas concentrations in the roof cavity and the lower container space for the sealed vents case. The Freon gas simulation reproduces the measurement in both the roof cavity and the container space reasonably well. This is true for both the magnitude of the gas concentrations as well as their time dependence. Wind speeds during 1 April were generally quite low – around 0.5 m/s except around mid-morning were a southerly briefly raised wind speeds to 2.5 m/s. This increased wind speed is evident in the drop in the gas concentration, especially in the roof cavity. A northerly wind with peak velocities of around 3.5 m/s was recorded in the second half of 2 April, again leading to a drop in the gas concentrations.

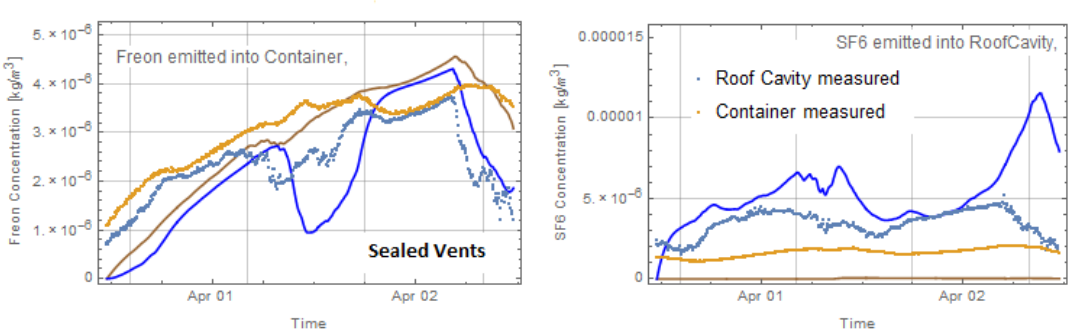

Figure 16. Measured (dots) and CONTAM simulation (line) of the Freon and SF6 gas concentrations in both zones of the skillion roof test set-up. Blue graphs refer to the roof cavity zone, while brown refers to the lower living space zone. The eaves vents were sealed in this case.

We have then opened three of the six vents on the northern and southern-facing eaves, doubling the SF_6 dosing rate into the roof cavity to 8 ml/min while retaining the Freon dosing rate into the container space. The mean wind speed was 1.6 m/s (maximum 6 m/s) with a predominantly northerly condition.

Figure 17 shows the comparison between measured data and CONTAM-simulated data using the airflow resistances from Table 3. The higher gas concentrations around 6 April coincide with the wind speed dropping below 1 m/s, thus reducing the air exchange in the test container set-up. Again, our simulation is in reasonable agreement with the measured data. The measured SF_6 concentration in the container space is, however, higher than the simulation for both the sealed and the open vents case, pointing to a transfer mechanism from the roof cavity to the container space, which is not perfectly captured in the model. While this needs further examination, the otherwise good correlation shows that our airflow resistances and *Cp* factors for the skillion roof set-up can be taken as a reasonable approximation of reality.

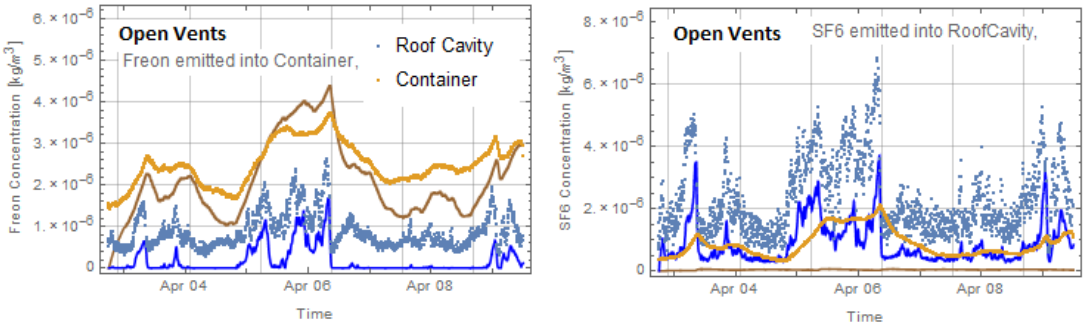

Figure 17. Measured (dots) and CONTAM-simulated (lines) gas concentrations for the vents open case.

3. Numerical simulation

This section describes the basis and the input parameters of the nodal model developed for this study. Actual results and discussion will be presented in the next section. The first subsection covers the climate source data as an input to the simulations. This is followed by a description of the nodal model and the materials properties used. We then describe the details of the nodal models for the two roof types investigated in this study (gable roof and skillion roof) as well as a model for the so-called baseline case. This refers to a hypothetical roof construct that is completely ventilated and will not have any interactions with the living space below.

3.1 Climate data and geographical locations

Simulations have been conducted for different locations and different seasons. Climate data for these simulations was obtained from NIWA, which has compiled Typical Meteorological Years (TMY) (Liley at al., 2007) data. In this study, we have used:

- AK – Auckland
- TP – Taupo/Turangi
- WN – Wellington
- CO – Central Otago.

Climate data consists of surface temperature [°C], absolute moisture content [g/kg], atmospheric pressure [Pa], wind speed at 10 m height [m/s], wind direction, cloud cover as well as global, diffuse and direct radiation [Wh/m^2]. The time resolution for the data is 1 hour, thus a yearly record will have 8,760 entries. Additional data needed for the simulations is derived from the NIWA data as best as possible. For instance, the simulation needs to take into account the long-wave radiation that is absorbed or emitted by the roof and, especially during a cloudy night, contributes to the energy flow balance.

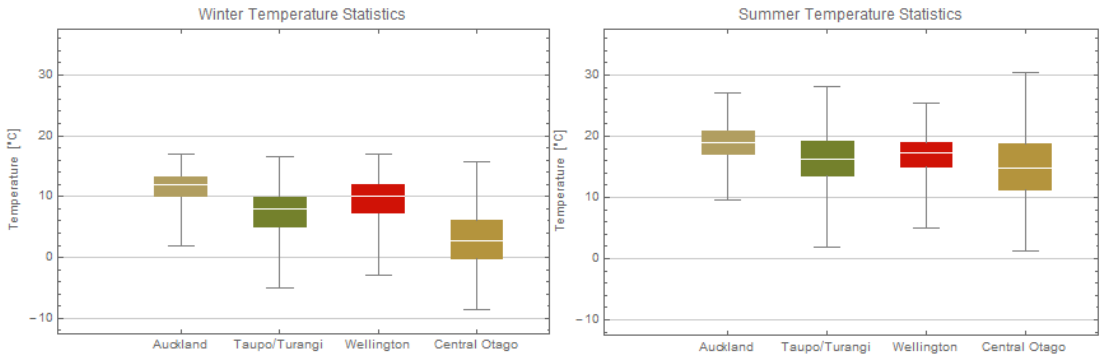

Figure 18. Winter and summer temperature statistics for the four climate zones. Displayed are maximum, 75% quantile, median, 25% quantile and minimum temperatures. Data by NIWA.

Cloud cover and temperature data provided by NIWA can be used to obtain this long-wave radiation following a formula described by the Fraunhofer Institute for Building Physics IBP (Kehrer, 2008). Basic psychrometric conversions such as absolute moisture to relative humidity are described in ASHRAE (2005). For our simulations, we have used winter and summer data only to cover the extreme situations in terms of temperature and humidity. Figure 18 summarises the winter and summer temperatures for the four zones as a statistical distribution.

The models use actual ambient temperature, relative humidity and radiation data using the available 1-hour time resolution for each geographical location. However, as described in the section on the nodal model, the wind speed and direction could not be incorporated into the nodal model on an hourly basis as the airflows throughout the building are a function of the wind parameters. At this stage, these airflows are calculated in CONTAM, as described above, and are an input to the nodal model. For the simulation, we used three different sets of steady airflows calculated in CONTAM for representative wind data.

The wind data used in the simulations for the four climate zones is listed in Table 4 and again derived from TMY data by NIWA. We have chosen to run simulations using the median, 25% and 75 % quantile wind speeds for the winter and summer months for the respective average wind directions.

Table 4. Wind speed statistics for the four climate zones used in this study. Given are the wind speeds in [m/s]. A value of 6.1 m/s in the 75% quantile bracket means that 25% of the recorded speeds are greater than 6.1 m/s. The data by NIWA is based on hourly averages.

	AK – Auckland		TP –Taupo/Turangi		WN – Wellington		CO– Central Otago	
	Summer	Winter	Summer	Winter	Summer	Winter	Summer	Winter
75%	6.1	6.6	4.6	3.7	6.6	5.1	5.4	2.7
Median	4.6	4.1	2.6	1.7	5.1	3.6	2.9	1.7
25%	2.5	2.0	1.5	1.1	3.0	2.0	1.7	1.2

Combining the four climate zones, two seasons and three wind speeds/direction, we arrive at 24 airflow calculations for each roof type. For each of these airflow parameters, a nodal model calculation is performed as described in the next sections. Table 5 summarises the CONTAM parameter matrix.

Table 5. Wind parameters as an input to the CONTAM building airflow calculation.

Location	Season	Wind Direction	Wind Speed	CONTAM BUILDING AIR FLOW CALCULATION	CONTAM Output: Building Air Flow
AUCKLAND	WINTER	Average - WINTER	75 % quantile		AK - WINTER - High Wind Speed
			Median		AK - WINTER - Median Wind Speed
			25% quantile		AK - WINTER - Low Wind Speed
	SUMMER	Average - SUMMER	75 % quantile		AK - SUMMER - High Wind Speed
			Median		AK - SUMMER - Median Wind Speed
			25% quantile		AK - SUMMER - Low Wind Speed
TAUPO/TURANGI	WINTER	Average - WINTER	75 % quantile		TP - WINTER - High Wind Speed
			Median		TP - WINTER - Median Wind Speed
			25% quantile		TP - WINTER - Low Wind Speed
	SUMMER	Average - SUMMER	75 % quantile		TP - SUMMER - High Wind Speed
			Median		TP- SUMMER - Median Wind Speed
			25% quantile		TP - SUMMER - Low Wind Speed
WELLINGTON	WINTER	Average - WINTER	75 % quantile		WN - WINTER - High Wind Speed
			Median		WN - WINTER - Median Wind Speed
			25% quantile		WN - WINTER - Low Wind Speed
	SUMMER	Average - SUMMER	75 % quantile		WN - SUMMER - High Wind Speed
			Median		WN- SUMMER - Median Wind Speed
			25% quantile		WN - SUMMER - Low Wind Speed
CENTRAL OTAGO	WINTER	Average - WINTER	75 % quantile		CO - WINTER - High Wind Speed
			Median		CO - WINTER - Median Wind Speed
			25% quantile		CO - WINTER - Low Wind Speed
	SUMMER	Average - SUMMER	75 % quantile		CO - SUMMER - High Wind Speed
			Median		CO- SUMMER - Median Wind Speed
			25% quantile		CO - SUMMER - Low Wind Speed

3.2 Nodal modelling

3.2.1 What is a nodal model?

In this context, a nodal model is an abstraction of building components and their physical properties and interaction onto a small number of points (nodes) and their connections (edges). It represents the bulk properties of building components or materials and their interaction with the surrounding. Property changes within the material or component are usually not considered. For example, if the top of a cladding has a temperature of 20°C and the bottom has one of 18°C, a single node will show the bulk material temperature of 19°C. This can only be overcome by introducing more nodes, in this example, a top node and a bottom node with a thermal resistance equal to that of the cladding material and its thickness. By adding more and more nodes, in principle, the model can be made arbitrarily complex, representing more and more aspects of the physical system. The nomenclature of nodes and edges is taken from graph theory because of the resemblance of nodal models with graphs.

The schematic in Figure 19 shows an example of how nodes are allocated to building components that make up the physical system under investigation. In this case, only one node is placed for each component. It is, however, also possible to place multiple nodes into one component in cases where a better special resolution is required.

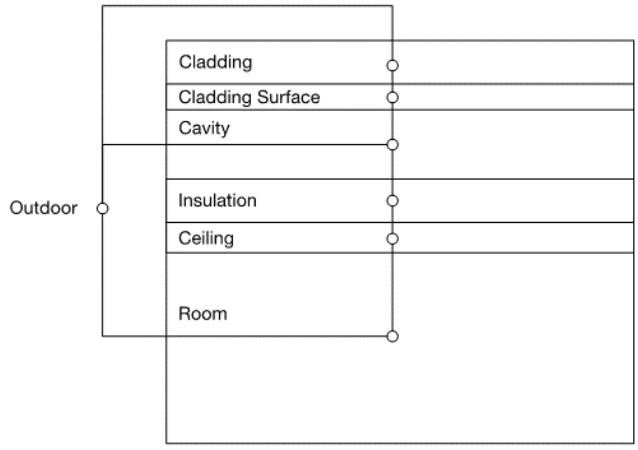

Figure 19. Nodes in building components describe the building as a physical system.

The nodal model as implemented for this research has the environment always in the first node, which then drives the temperature and humidities of the other nodes according to their transport resistances and so on. The implementation of the nodal model allows driving the temperature of other nodes by means of an interpolation function, which is then used instead of the initial temperature value. This means, however, that this node's temperature will not be solved for but is replaced by the value set by the interpolation function. The humidity of the nodes cannot be set via an interpolation function in this implementation but needs to be solved for. In case the humidity for a node needs to be altered over time, a moisture source/sink needs to be declared for that node.

Figure 20 shows a small detail of a roof nodal model as represented within Mathematica. The points represent the nodes and are material properties, while the lines (edges) represent the resistances or conductances between the nodes. The use of the nodal model is not restricted to the application in building physics. It can be applied to the solution of many dynamic systems in which the bulk properties of components and their interaction need to be modelled.

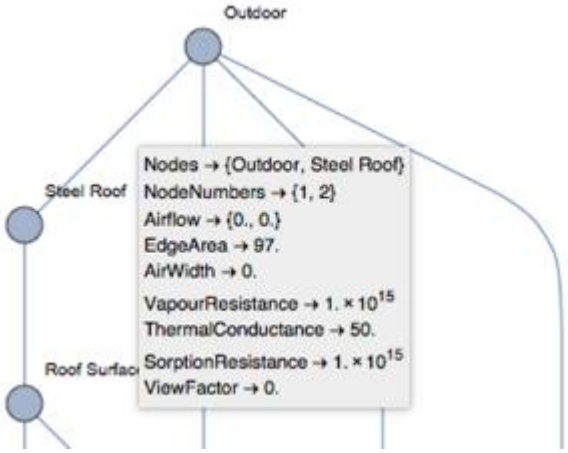

Figure 20. Section of the graphical representation of a nodal model with an edge property overlay.

As with any modelling and simulation, it is good practice to have a benchmark against which the performance of a model can be assessed. Benchmarking helps to avoid creating models that cannot replicate measurements conducted on real buildings or building components. It allows the model to be fine tuned to reflect reality as close as possible given the resolution of the model. Once the benchmarking has been done, model parameter changes, for example, changes in outdoor climate, can then simulate how the building would perform under conditions that are different to those at the time of the measurement.

3.2.2 Nodal model mathematics

In this section, mathematical formulas used to describe the nodal model are presented and described. The equations are describing a coupled system of first order differential equation that need to be solved simultaneously. For each node, there is one mass and one heat equation describing the properties and flows of heat, air and moisture to and from that node. The symbols used in the equations are described in Table 6.

Table 6. Symbols used in the nodal model equations.

Symbol	Unit	Comment
A_{ij}	m^2	Area between nodes i and j
c_i	J/kg K	Specific heat of material at node i
c_p	J/m^3 K	Specific heat of air at constant pressure
F_{ij}	m^3/s	Air exchange rate from node i to node j
h_{vij}	W/m^2K	
L_{ij}	J/kg	Latent heat
m_i	kg/m^3	Vapour density
m_i'	kg/m^3	Vapour density at next time step
p_i	Pa	Water vapour pressure at node i
r_{ij}	Ns/kg	Water vapour transport resistance between nodes i and j
ρi	kg/m^3	Material density of node i
ϑ_i	kg/m^3	Concentration of condensate in node i
t	s	Time
T_i	K	Temperature at node i
U_{ij}		Thermal conductance between nodes i and j
V_i	m^3	Volume of node i

The model solves the mass equation [Eq3] for vapour density, that is, kilograms of water per cubic metre of material that is represented by the node. The rate of change in vapour density at node *i* is driven by the vapour pressure difference between node *i* and all other nodes in the system plus the net inflow of moist air from other nodes and the flow attributed to convection. Details of the derivation of the governing equation can be found in Cunningham (1980).

$$V_i\left(\frac{m_i' - m_i}{\Delta \mathrm{t}}\right) = \sum_j \left(A_{\mathrm{ij}} \frac{p_j' - p_i'}{r_{\mathrm{ij}}} + V_i\left(F_{\mathrm{ji}}^i m_j' - F_{\mathrm{ij}}^i m_i'\right) + A_{\mathrm{ij}} h_{v_{\mathrm{ij}}}\left(p_j' - p_i'\right) \right) \quad \text{[Eq3]}$$

The energy flow is governed by Equation [Eq4], where the rate of change in temperature at node *i* depends on the temperature difference and the thermal conductance between node *i* and all other nodes, the infiltration and exfiltration of air and the latent heat of evaporating or condensating moisture.

$$p_i c_i V_i\left(\frac{r_i' - r_i}{\Delta t}\right) = \sum_j \left(A_{ij} U_{ij}\left(T_j' - T_i'\right) + c_p V_i\left(F_{ji}^i T_j' - F_{ij}^i T_i'\right)\right) + V_j L_{ij}\left(\frac{\Delta \vartheta_i}{\Delta t}\right) \quad \text{[Eq4]}$$

The term $\frac{\Delta \vartheta_i}{\Delta \mathrm{t}}$ in Equation [Eq4] represents the amount of condensate/evaporate that has been accumulated during the time step Δt. This amount can be written as follows:

$$\frac{\Delta \vartheta_i}{\Delta \mathrm{t}} = \frac{d(m - m_{sat})}{dt} \quad \text{[Eq5]}$$

The saturation vapour density depends only on the temperature of the node so that the equation can be rewritten in a form that allows easier calculation:

$$\frac{d(m - m_{\mathrm{sat}})}{\mathrm{dt}} = \frac{dm}{dt} - \frac{dm_{sat}}{dT}\frac{dT}{dt} \quad \text{[Eq6]}$$

With this, the energy equation can be rewritten to

$$\frac{dT_i}{dt} = \frac{\sum_j \left(A_{\mathrm{ij}} U_{\mathrm{ij}}\left(T_j' - T_i'\right) + c_p V_i\left(F_{\mathrm{ji}}^i T_j' - F_{\mathrm{ij}}^i T_i'\right)\right) + V_i L_{ij}\frac{dm_i}{dt}}{\rho_i c_i V_i + V_i L_{ij}\frac{dm_{sat}}{dT}} \quad \text{[Eq7]}$$

Each node contains the properties of the material that the node is going to represent in the simulation such as heat capacity, density, emissivity, volume and radiative area as well as the initial conditions of temperature and humidity.

3.3 Materials and resistances

Table 7 below lists all materials and their properties used in the nodal models described later in this document.

Table 7. General materials properties used in the nodal model simulations.

Material	Vapour permeability [kg/m s Pa]	Thermal conductivity [W/m K]	Density [kg/m3]	Heat Capacity [J/ kg K]
Air	$2*10^{-10}$	0.0257	1.2	1005
Steel	10^{-20}	45	7860	420
Wood	–	0.1	500	2500
Gypsum board	$4.2*10^{-11}$	0.17	800	1090
Fibreglass	$150.94*10^{-12}$	0.0473	16	848

3.4 Input parameters

Apart from the initial relative humidity and the temperature conditions at each node, the nodal model requires the input parameters as shown in Table 8

Table 8. Input parameters to the nodal model simulations.

Parameter	Comment
Outdoor relative humidity	Obtained from NIWA TMY files for the location of interest
Outdoor temperature	
Outdoor diffuse and direct solar radiation	
Indoor temperature	This can either be calculated by the model by setting an initial value or can be set via an interpolation function
Indoor heating	This is usually a constant in W/s
Indoor moisture source rate	A constant production rate of moisture in kg/s
Air infiltration	The air infiltration into the various cavities is usually set to be a constant that was calculated using a CONTAM simulation

3.5 Sky radiation model

The sky radiation model that is used in the nodal models has been derived from the one that is used by WUFI 4.0. More details can be found at www.wufi-wiki.com/mediawiki/index.php5/Details:LongWaveExchange.

3.6 Undercooling

This is an important but often overlooked effect that has a stark impact on the moisture tolerance of roofs. Undercooling arises from the radiant heat exchange between the roof surface, the terrestrial environment and the sky. The sky absorbs all radiation that is coming from the surface but emits radiation only anisotropically at a selected wavelength. This causes the outside roof surface to cool down below the ambient air temperature and thus possibly below the dew point of the outside air. This temperature drop is most prominent in windless conditions for surfaces with high emissivity that fully face the clear sky. The reason is that the convective surface coefficient will drop to low values allowing an effective cooling of the surface to take place. This effect takes place predominantly during the night in clear sky conditions but can also be observed during the day in certain locations in winter (Cunningham, 1980).

An outdoor relative humidity of 100% is rarely observed and not present in the climate data we have used in this open roof model. The condensation conditions are therefore arising solely due to night-time radiative undercooling. Figure 21 shows how much the roof surface of the open roof is cooled below ambient temperature for the locations Auckland, Taupo, Wellington and Central Otago and the Typical Meteorological Year climate data used in the simulation.

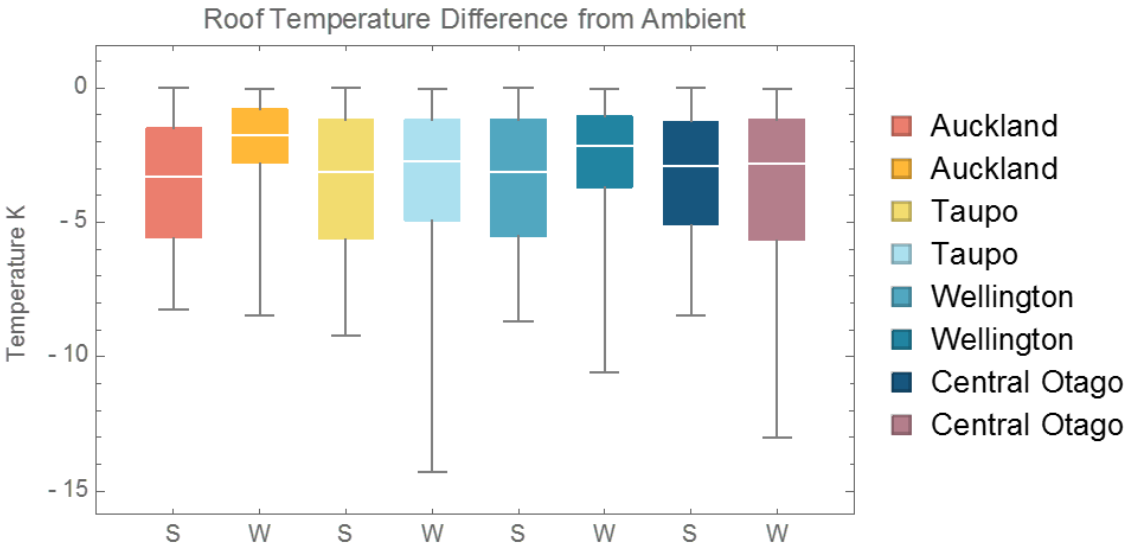

Figure 21. Cooling potential below ambient temperatures at various locations during the summer (S) and winter (W) months.

3.7 Model description – open steel roof

The model is a rather simple nodal model with just four nodes: outdoor, steel cladding, cladding surface and ground. The roof surface area was set to 100 m^2.

Table 9. Properties of the open steel roof nodes.

Node name	Properties	
Outdoor	Temperature:	climate data
	Water vapour density:	climate data
Steel cladding	Initial temperature:	same as ambient
	Water vapour density:	0.0
	Volume:	1 mm * roof surface area
	Area:	roof surface area
	Specific heat:	420 J/kg K
	Density:	7860 kg/m^3
	Receives sky radiation:	true
Cladding surface	Initial temperature:	same as ambient
	Initial water vapour density:	same as ambient
	Volume:	1 mm * roof surface area
	Area:	roof surface area
	Specific heat:	1005 J/kg K
	Density:	1.205 kg/m^3
	Emissivity:	0.8
Ground	Initial temperature:	same as ambient
	The ground node was there to form a source of radiative heat exchanged with the cladding surface.	

The nodes are connected with four so-called edges that are describing the exchange of heat, moisture and radiation.

Table 10. Interconnection properties between the nodes in the open steel roof nodal model.

Connection	Properties	
Outdoor – steel cladding	Area: Vapour resistance: Thermal conductance:	roof surface area infinite 50 W/K
Steel cladding – cladding surface	Area: Vapour resistance: Thermal conductance:	roof surface area infinite 20 W/K
Outdoor – cladding surface	Area: Air width: Vapour resistance: Thermal conductance:	roof surface area 0.3 (convection term) 750*108 N s/Pa 0.0257 W/m K * 0.3m
Steel cladding – ground	View factor:	9.848, 9.848, 0.3 parameters for factor calculation (see Mathematica file: OpenSteelRoof.nb)

While the outdoor, steel cladding and ground nodes are straightforward entities of the roof, the cladding surface node has been introduced to model a ground-facing 1mm thick boundary layer of the cladding in order to calculate the condensation condition close to the steel cladding.

The nodal model will store any condensate in this node, and this is from where condensate will be evaporated. In this simple model, the evaporated moisture will be released into the outdoor environment, which is an infinite source/sink of moisture and will not show up in any node of the model.

The model is run with four climate files derived from the NIWA TMY files for Auckland, Taupo/Turangi, Wellington and Central Otago. Only the summer months (1/12 to 28/02) and the winter months (01/06 to 31/08) where used in the simulation in order to be comparable with other simulations and to keep the calculation time at a manageable level.

In the analysis of the simulation results, we calculated the number of hours condensation conditions for the roof cladding were present and the number of hours condensate was present on the cladding (wetness hours). The results are discussed in section 4.1.

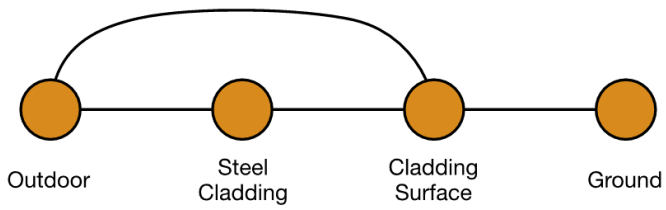

Figure 22: Open steel roof model outline of nodes and their interconnections.

3.8 Model description – gable Roof

As mentioned above, the gable roof model was implemented in conjunction with measurements conducted in a 60 m^2 home in National Park that serves as a benchmark against which the performance of the gable roof model is evaluated. The measurements and the relevant details of the house are described in section 0.

The properties relevant to the model are listed in Table 11 below.

Table 11. Dimensions of the gable roof building at National Park.

Component name	Size
Roof surface area	97.0 m^2
Cavity volume	30.6 m^3
Insulation volume	13.4 m^3
Roof cavity floor area	89.3 m^2
Indoor wall area	94.0 m^2
Indoor volume	140.0 m^3

The intention of this model is to determine the heat, air and moisture balance of a gable roof in different locations in New Zealand. The model roof is constructed above a single-zone room with wall and ceiling insulation equivalent to R2.8. The ceiling is covered in gypsum plasterboard with fibreglass as insulation material.

The attic has a volume of 44 m^3, and the steel roof cladding has an area of 97 m^2.

The roof ridge of the benchmark building is oriented along the north-south direction, while the model roof has no orientation, as we are mostly interested in the impact of night-time radiation, which is uniform over the night-time sky. Hence, the roof was placed in the model horizontally with a tilt angle of 0 degrees. The azimuth of the roof need then not to be considered and is set to 0 too.

Modelling the directionality of the roof would have been possible but would have complicated the model and the calculation time with little to no gain.

The hourly means of temperature, relative humidity and long-wave and short-wave radiation for each location is taken from NIWA typical mean climate data files and used as input parameters for the outdoor node of the model. The sky radiation is used to calculate the night-time cooling of the surfaces that are 'seeing' the sky, which is only the roof cladding in this model.

The indoor temperature was set to a constant, and setting the indoor temperature to 289, 291, 293 and 295 Kelvin, respectively, simulated the effect of the indoor temperature on the roof cladding condensation hours. The radiative heat exchange between the cladding surface and the ceiling insulation top was simulated by assuming that the emissivity for both surfaces is 0.8. The view factor for theses surfaces was calculated by assuming that the roof is an equilateral triangle.

The model consists of 7 nodes and 11 interaction connections as shown in Figure 23.

Nodes have been implemented for the elements given in Table 12.

Table 12. Nodes for the gable roof model

Node name	Properties	
Outdoor	Temperature:	climate data
	Water vapour density:	climate Data
Steel cladding	Initial temperature:	same as ambient
	Water vapour density:	0.0
	Volume:	1 mm * roof surface area
	Area:	roof surface area
	Specific heat:	420 J/kg K
	Density:	7860 kg/m^3
	Receives sky radiation:	true
Cladding surface	Initial temperature:	same as ambient
	Initial water vapour density:	same as ambient
	Volume:	1 mm * roof surface area
	Area:	roof surface area
	Specific heat:	1005 J/kg K
	Density:	1.205 kg/m^3
	Emissivity:	0.8 (estimated)
Air cavity	Initial temperature:	estimate
	Initial water vapour density:	estimated 0.7 of saturation vapour density
	Volume:	30.6 m^3
	Specific heat:	1005 J/kg K
	Density:	1.205 kg/m^3
Timber	Initial temperature:	cavity air temperature
	Initial water vapour density:	estimated 0.5 of saturation vapour density
	Volume:	1.1 m^3
	Specific heat:	2500 J/kg K
	Density:	420 kg/m^3
	Sorption function:	pine
Ceiling	Initial temperature:	estimated from ambient and indoor
	Initial water vapour density:	estimate 0.7 of saturation vapour density
	Volume:	13.4 m^3
	Specific heat:	848 J/kg K
	Density:	16 kg/m^3
	Emissivity:	0.8 (estimated)
Indoor	Initial temperature:	constant 293 K
	Initial water vapour density:	estimated 0.5 of saturation vapour density
	Constant moisture source:	72 g/h (approx. 1 person)
	Volume:	140 m^3
	Specific heat:	1005 J/kg K
	Density:	1.205 kg/m^3

The 7 nodes are connected with 11 edges that are describing the exchange of heat, moisture and radiation (Table 13)

Table 13. Nodal interconnection properties.

Connection	Properties	
Outdoor – indoor	Area:	indoor wall + floor area
	Vapour resistance:	infinite
	Thermal conductance:	0.357 W/K (R2.8)
	Airflow:	according to simulation schedule
Outdoor – steel cladding	Area:	roof surface area
	Vapour resistance:	infinite
	Thermal conductance:	50 W/K
Outdoor – timber	Area:	10.4 m^2
	Vapour resistance:	infinite
	Thermal conductance:	10 W/K
Outdoor – cavity	Area:	82.5
	Vapour resistance:	infinite
	Airflow:	according to simulation schedule
Cladding surface – steel cladding	Area:	roof surface area
	Vapour resistance:	infinite
	Thermal conductance:	20 W/K
Cladding surface – ceiling	Area:	roof surface area
	Vapour resistance:	infinite
	View factor:	9.48, 9.48, 0.5
Cavity – cladding surface	Area:	roof surface area
	Vapour resistance:	1.6*1010 N s/Pa
	Thermal conductance:	0.008 W/K
	Air gap:	0.3 m (convection distance)
Cavity – indoor	Airflow:	according to simulation schedule
Cavity – timber	Area:	39.6 m^2
	Vapour resistance:	750*106 N s/Pa
	Thermal conductance:	19 W/K
	Sorption resistance:	1.83*107 s/m
Ceiling – cavity	Area:	89.3 m^2
	Vapour resistance:	1.6*1010 N s/Pa
	Thermal conductance:	0.008 W/K
	Air gap:	0.2 m (convection distance)
Ceiling – indoor	Area:	89.3 m^2
	Vapour resistance:	2.26*106 N s/Pa
	Thermal conductance:	0.357 W/K

The vapour resistance between the outdoor and the indoor node is set to infinity as the diffusion process is very slow and will not contribute much given the high air exchange between outdoor and indoor. The air exchanges between the various nodes are set according to the simulation results obtained through CONTAM and taken from the simulation schedule for winter and summer climatic conditions.

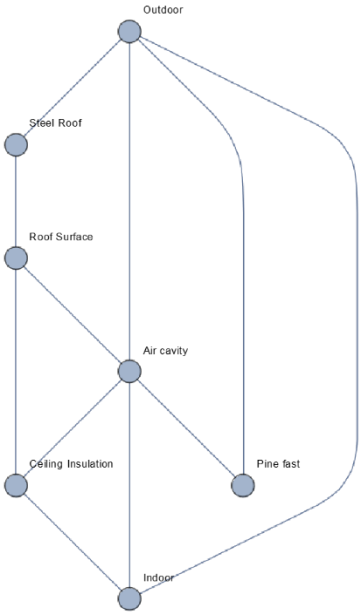

Figure 23. Sketch of the gable and skillion roof nodes and their interconnections.

3.9 Model description – skillion roof

The skillion roof constructed above a shipping container located on the BRANZ campus has been used to run roof performance experiments by measuring air infiltration, temperature and moisture levels at various locations in the roof and the room underneath. The measurements were used to develop a CONTAM model to calculate air infiltration at given wind conditions. This air infiltration data together with the temperatures and moisture levels are then used to benchmark a nodal model that is described in the forthcoming sections.

Table 14. Dimensions of the skillion roof test container.

Component name	Size
Roof surface area	31.0 m^2
Cavity volume	2.0 m^3
Timber area (cavity facing)	9.0 m^2
Timber area (roof facing)	1.8 m^2
Timber volume (above insulation)	0.14 m^3
Timber volume (at insulation)	0.48 m^3
Insulation volume	4.6 m^3
Indoor floor/ceiling area	30.0 m^2
Indoor wall area	79.8 m^2
Indoor volume	85.0 m^3

The environmental conditions are taken from four locations in New Zealand – Auckland, Taupo/Turangi, Wellington and Central Otago. The settings were assumed to be rural. Most conditions and parameters are the same as those for the gable roof model. The indoor temperature was set to 293 Kelvin and not varied, as the results obtained during the gable roof model runs are transferable to the skillion roof and the calculation time of the skillion roof model was very long due to prolonged condensation events and a parameter variation would have caused excessive delays.

The model consists, as for the gable roof model, of 7 nodes and 11 interaction connections as shown in Figure 23. Nodes have been implemented for the elements given in Table 15.

Table 15. Nodes for the skillion roof model.

Node name	Properties	
Outdoor	Temperature:	climate data
	Water vapour density:	climate Data
Steel cladding	Initial temperature:	same as ambient
	Water vapour density:	0.0
	Volume:	1 mm * roof surface area
	Area:	roof surface area
	Specific heat:	420 J/kg K
	Density:	7860 kg/m^3
	Receives sky radiation:	true
Cladding surface	Initial temperature:	same as ambient
	Initial water vapour density:	same as ambient
	Volume:	1 mm * roof surface area
	Area:	roof surface area
	Specific heat:	1005 J/kg K
	Density:	1.205 kg/m^3
	Emissivity:	0.8 (estimated)
Air cavity	Initial temperature:	estimate
	Initial water vapour density:	estimated 0.7 of saturation vapour density
	Volume:	2.0 m^3
	Specific heat:	1005 J/kg K
	Density:	1.205 kg/m^3
Timber	Initial temperature:	cavity air temperature
	Initial water vapour density:	estimated 0.5 of saturation vapour density
	Volume:	0.14 m^3
	Specific heat:	2500 J/kg K
	Density:	420 kg/m^3
	Sorption function:	pine
Ceiling	Initial temperature:	estimated from ambient and indoor
	Initial water vapour density:	estimate 0.7 of saturation vapour density
	Volume:	4.6 m^3
	Specific heat:	848 J/kg K
	Density:	16 kg/m^3
	Emissivity:	0.8 (estimated)
Indoor	Initial temperature:	constant 293 K
	Initial water vapour density:	estimated 0.5 of saturation vapour density
	Constant moisture source:	72 g/h (approx. 1 person)
	Volume:	85 m^3
	Specific heat:	1005 J/kg K
	Density:	1.205 kg/m^3

The 7 nodes are connected with 11 edges that are describing the exchange of heat, moisture and radiation (Table 16).

Table 16. Interconnections between the skillion roof nodes.

Connection	Properties	
Outdoor – indoor	Area:	indoor wall + floor area
	Vapour resistance:	infinite
	Thermal conductance:	0.357 W/K (R2.8)
	Airflow:	according to simulation schedule
Outdoor – steel cladding	Area:	roof surface area
	Vapour resistance:	infinite
	Thermal conductance:	50 W/K
Outdoor – timber	Area:	1.8 m^2
	Vapour resistance:	infinite
	Thermal conductance:	10 W/K
Outdoor – cavity	Area:	31.0 m^2
	Vapour resistance:	infinite
	Airflow:	according to simulation schedule
Cladding surface – steel cladding	Area:	31.0 m^2
	Vapour resistance:	infinite
	Thermal conductance:	20 W/K
Cladding surface – ceiling	Area:	31.0 m^2
	Vapour resistance:	infinite
	View factor:	5.43, 5.43, 0.06
Cavity – cladding surface	Area:	31.0 m^2
	Vapour resistance:	3.25*106 N s/Pa
	Thermal conductance:	0.086 W/K
	Air gap:	0 m (no convection)
Cavity – indoor	Airflow:	according to simulation schedule
Cavity – timber	Area:	9.0 m^2
	Vapour resistance:	750*106 N s/Pa
	Thermal conductance:	0.4 W/K
	Sorption resistance:	1.83*107 s/m
Ceiling – cavity	Area:	30.0 m^2
	Vapour resistance:	3.25*106 N s/Pa
	Thermal conductance:	0.4 W/K
	Air gap:	0 m (no convection)
Ceiling – indoor	Area:	30.0 m^2
	Vapour resistance:	626*107 N s/Pa
	Thermal conductance:	0.357 W/K

4. Results

The results in this section are not to be interpreted as absolute figures but should be used to illustrate relative differences, for example, they are useful to compare sealed and opened vent configurations or different wind speeds and geographical zones. While the model is of course capable of producing accurate absolute figures, this will require absolute accuracy of all the input parameters, which is not always possible.

4.1 Baseline model – open steel roof

As mentioned in the introduction, it is educative to look at an ideally ventilated roof cavity in comparison to a roof cavity that is maintained at an indoor climate – an ideal warm roof.

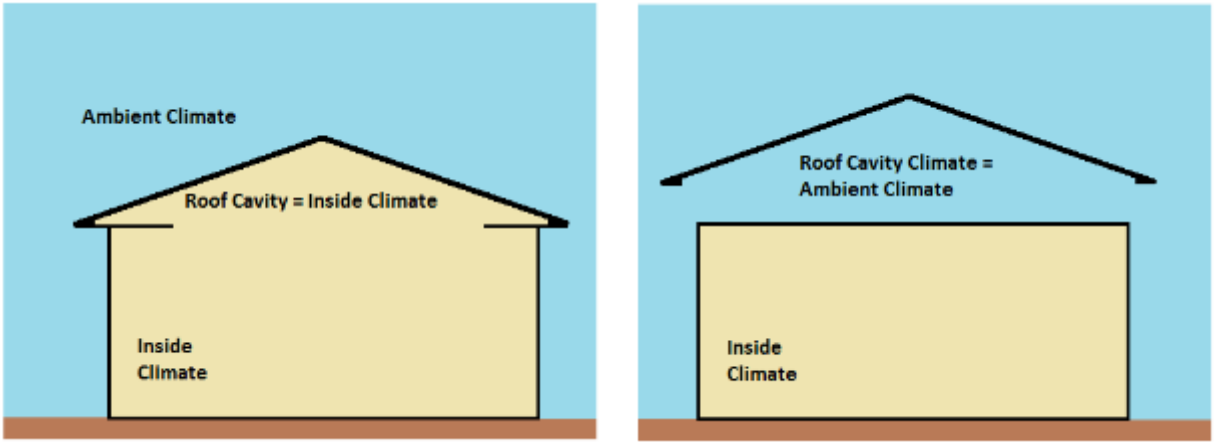

Figure 24. Idealisation of a warm roof and a ideally ventilated roof cavity.

The ideal warm roof situation on the left in Figure 24 has the roof cavity climate equal to the inside climate. All surfaces in the roof cavity are maintained at the inside temperature even though radiative cooling can drop the outside roof surface to below ambient temperature.[7] As long as the inside climate itself does not reach the dew point temperature, no condensation will occur in the roof cavity.

On the other hand, if we look at a ideally or completely ventilated roof, the temperature and humidity in the roof cavity will be the same as the outside conditions. The ceiling level of the building is then absolutely airtight and ideally thermally insulated, meaning that no moisture or heat exchange is present between the two zones. The roofing iron itself can now reach lower temperatures on either side due again to the radiative cooling into a clear night sky. The underside of the iron will gain some energy from a radiative exchange with the ceiling. We have simulated this ideally ventilated case for our four climate zones – Auckland, Taupo/Turangi, Wellington and Central Otago. For each climate zone, we compare the three summer and winter months only.

Table 17 summarises the results of the ideally ventilated roof model. We distinguish between the condensation condition and the wetness condition – the former is simply

[7] A temperature gradient then exists across the roofing iron, leading to heat flux and energy loss, which needs to be compensated by heating.

based on the dew point temperature. Once this temperature is reached within the time resolution of the model (1 hour), this time is counted.

The wetness condition takes into account the fact that, after the condensation condition is no longer valid, it will take time for any water formed on the surface to evaporate again. Thus, the condensation condition will generally be shorter than the wetness condition. However, the latter will be more significant when it comes to adverse effects to the elements of the building.

Table 17. Percentage of time the underside of roofing cladding of an ideally ventilated roof cavity will be in a condensation or wetness condition.

Location	Summer (Dec, Jan, Feb)	Winter (Jun, Jul, Aug)	Summer	Winter
	Condensation condition		Wetness condition	
Auckland	0.7 %	6 %	1 %	8 %
Taupo/Turangi	5 %	20 %	7 %	20 %
Wellington	2 %	3 %	3 %	4 %
Central Otago	7 %	10 %	10 %	20 %

As expected, the winter months yield higher condensation and wetness percentages than the summer months, due to the lower temperatures. We can further see a significant geographical influence. While the climate zones of Taupo/Turangi and Central Otago, with the lower winter temperatures, reach condensation condition percentages of 20% and 10% respectively, the milder zones of Auckland and Wellington remain in the single-digit percentages. Wetness condition percentages are usually longer than condensation conditions with the exception of the Taupo/Turangi zone in winter.

4.2 Gable roof

The results of the numerical simulation for the gable and skillion roof can be given in different ways. As stated above, at this stage, we cannot simulate a complete year with the time-resolved airflow changes throughout the building as a function of the external climate changes. The results for winter and summer and the three statistical wind speed conditions for each of the four geographical zones are summarised in Table 18. The two configurations with the roof cavity vents sealed and open are compared. First, our modelling points to more condensation events during the winter months, which is to be expected. This is true for all the climate zones, wind conditions and vent configurations. We also find significant difference in the climate zones. Auckland exhibits some of the greatest condensation event percentages, which can be attributed partially to the high atmospheric moisture content. The Auckland climate zone has the highest mean annual moisture content of 8.5 g water per kilogram of dry air followed by Wellington (7.4 g/kg), Taupo/Turangi (7.1 g/kg) and Central Otago with the lowest value of 5.2 g/kg. In general, we also observe a decrease in the condensation condition events with increasing wind speed. The increased wind speed results in higher infiltration rates in the roof cavity exchanging some moisture air from downstairs with drier air. Beyond a certain wind speed condition, this beneficial effect is exhausted, and the condensation condition events do not fall any further. We approach the baseline regime described in the previous section. Essentially, any moist indoor air has been removed. However, the conditions are such that the ambient air itself, aided by the undercooling effect of the roof, has driven the ambient air below the dew point temperature.

Table 18. Percentage of time the gable roof cavity will be in a condensation condition. Closed and open vents configurations are given.

Location	Wind speed quantile	Condensation condition			
		Summer	Winter	Summer	Winter
		Sealed		Open	
Auckland	25%	47%	69%	1%	6%
	50%	16%	30%	1%	6%
	75%	11%	20%	1%	6%
Taupo/Turangi	25%	8%	24%	5%	16%
	50%	7%	20%	5%	14%
	75%	6%	18%	5%	14%
Wellington	25%	8%	17%	2%	3%
	50%	3%	8%	2%	3%
	75%	2%	6%	2%	3%
Central Otago	25%	12%	20%	8%	12%
	50%	10%	17%	8%	12%
	75%	12%	14%	7%	11%

A careful comparison between Table 17 and Table 18 shows that some condensation event percentages for the ideally ventilated (completely open) baseline case are worse than for the less ventilated gable roof case. For instance, for the Taupo/Turangi climate zone, we find a 20% probability of a condensation event during the winter months in the baseline model, while our ventilated gable roof building yields slightly better values between 14% and 16%. This is due to the fact that the temperature in the gable roof cavity is higher than the outside temperature due to the non-perfect ceiling insulation. Thus, this higher temperature in the cavity prevents some of the condensation events.

Clear benefits can be seen when the roof cavity vents are opened. We see a reduction in the condensation event percentages for all climate zones and wind conditions.

The following figures are aimed at illustrating the simulation results in more detail. Here, we plot the probability of condensation duration. In other words, if the condensation criterion is reached, the histograms indicate the probability of how long this condition will last for.

Again, we distinguish between the four climate zones, two seasons and the wind speed quantiles. Looking at Figure 27, for instance, we can see how opening the vents would have a significant effect on the condensation event length in the Auckland climate zone. Especially when we assume the lower wind speed condition (25% quantile), we find a high probability of these events lasting for anywhere between 15 and 20 hours. Opening the vents shifts these probabilities towards the shorter duration spectrum.

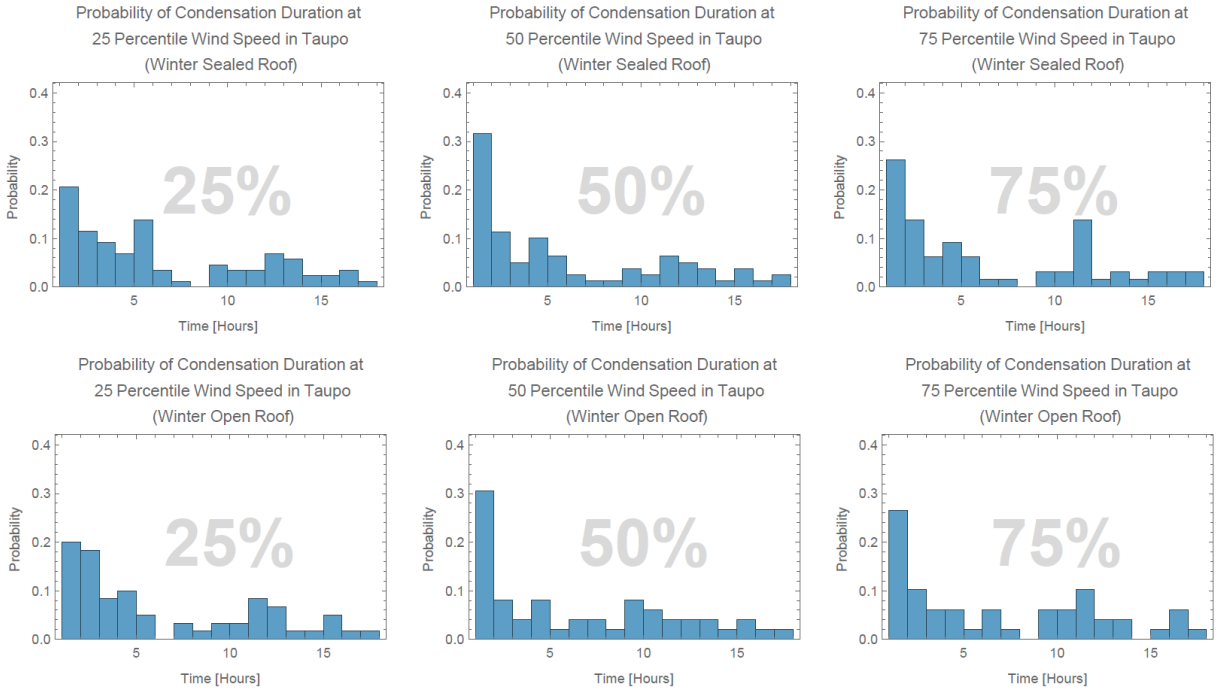

Figure 25. Condensation statistics for the gable roof in the Taupo/Turangi zone for the winter months and the three wind speeds: comparison between open and closed vents.

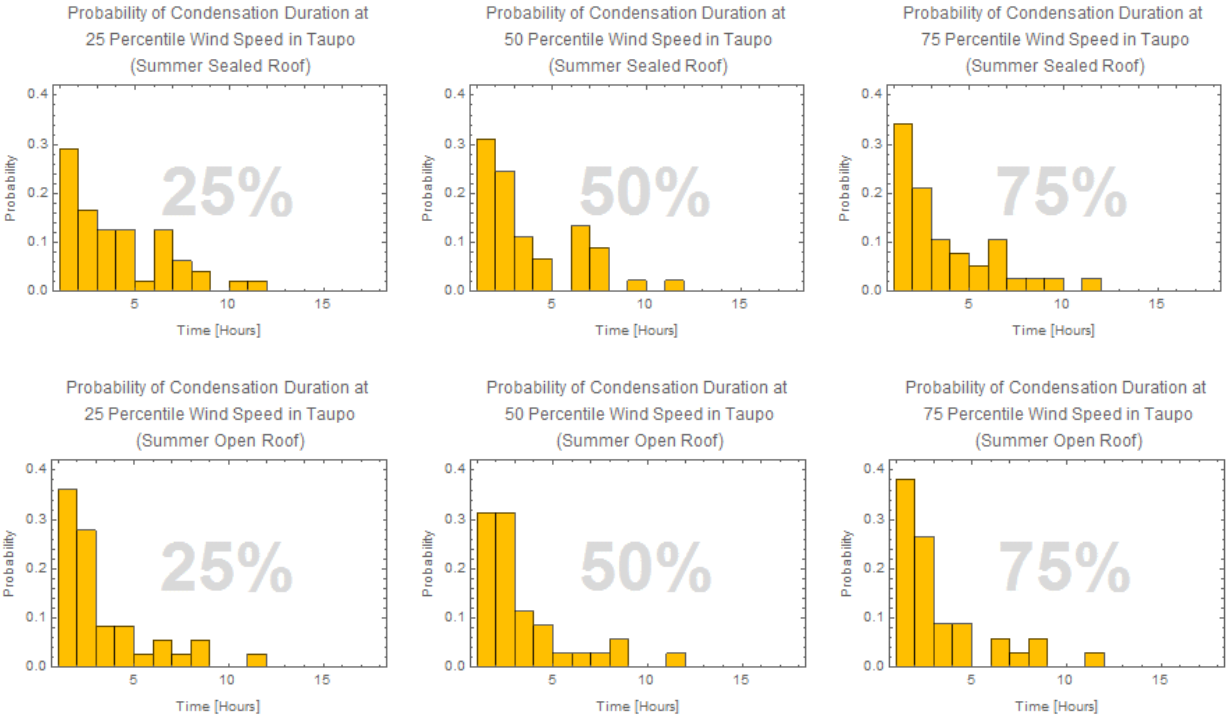

Figure 26. Condensation statistics for the gable roof in the Taupo/Turangi zone for the summer months and the three wind speeds: comparison between open and closed vents.

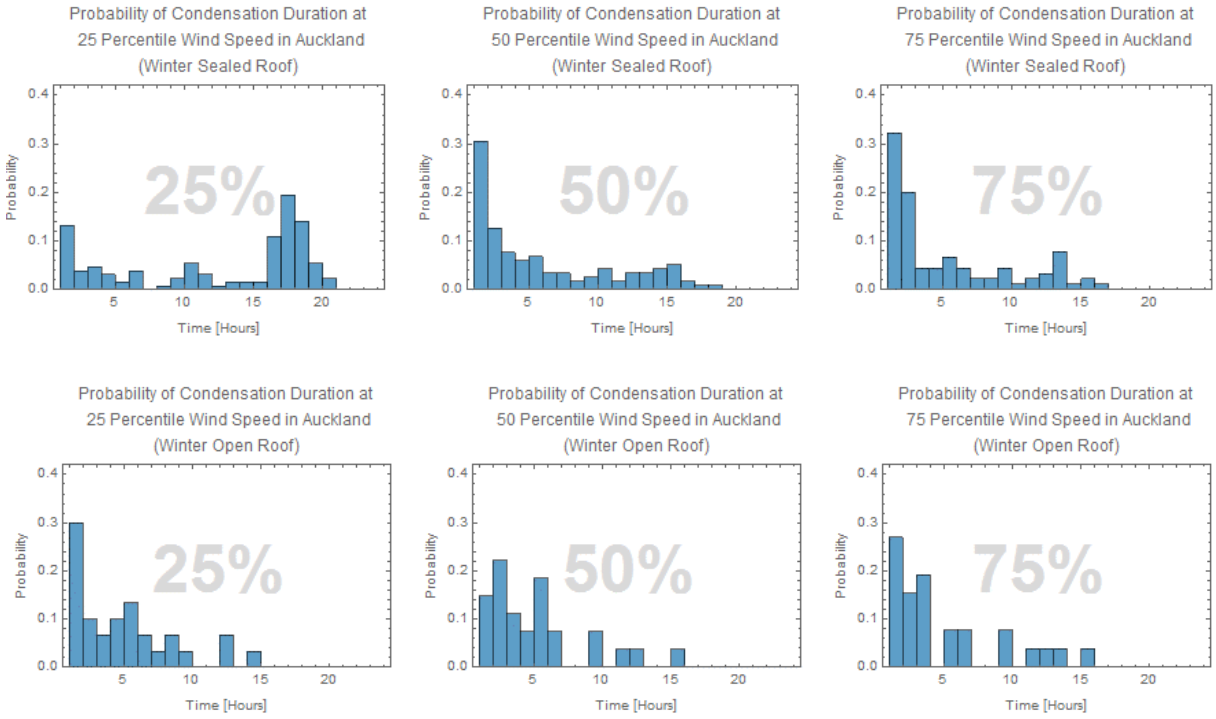

Figure 27. Condensation statistics for the gable roof in the Auckland zone for the winter months and the three wind speeds: comparison between open and closed vents.

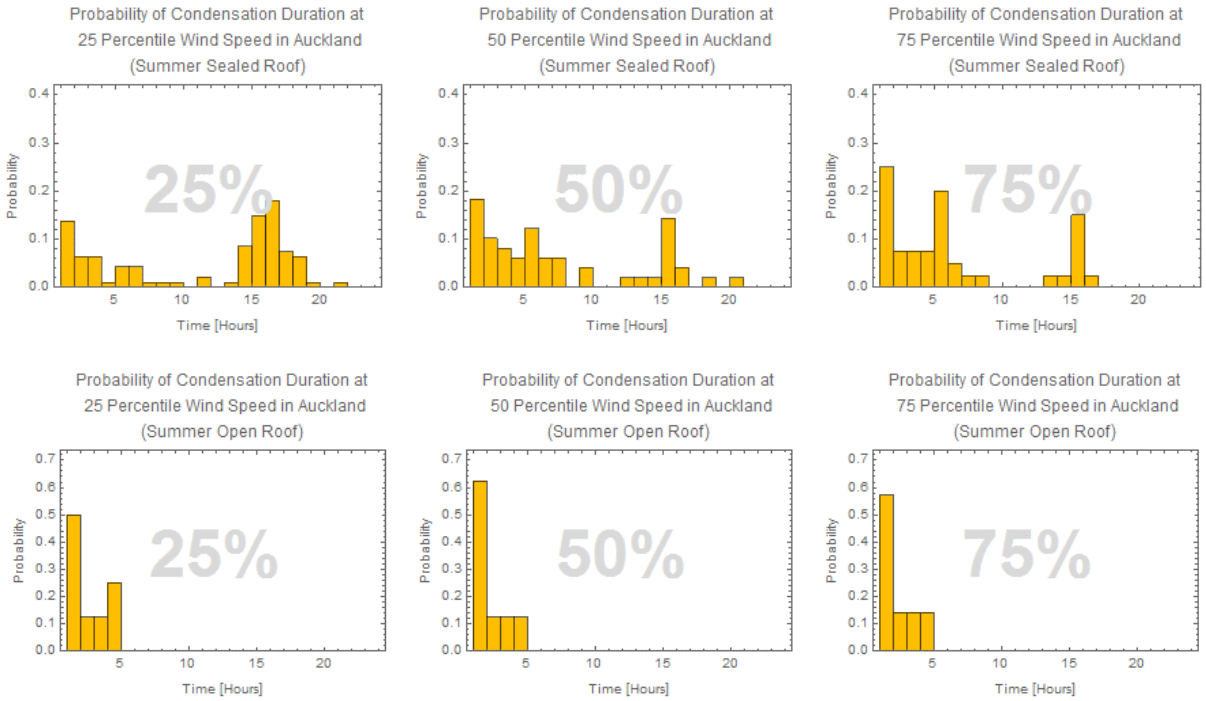

Figure 28. Condensation statistics for the gable roof in the Auckland zone for the summer months and the three wind speeds: comparison between open and closed vents.

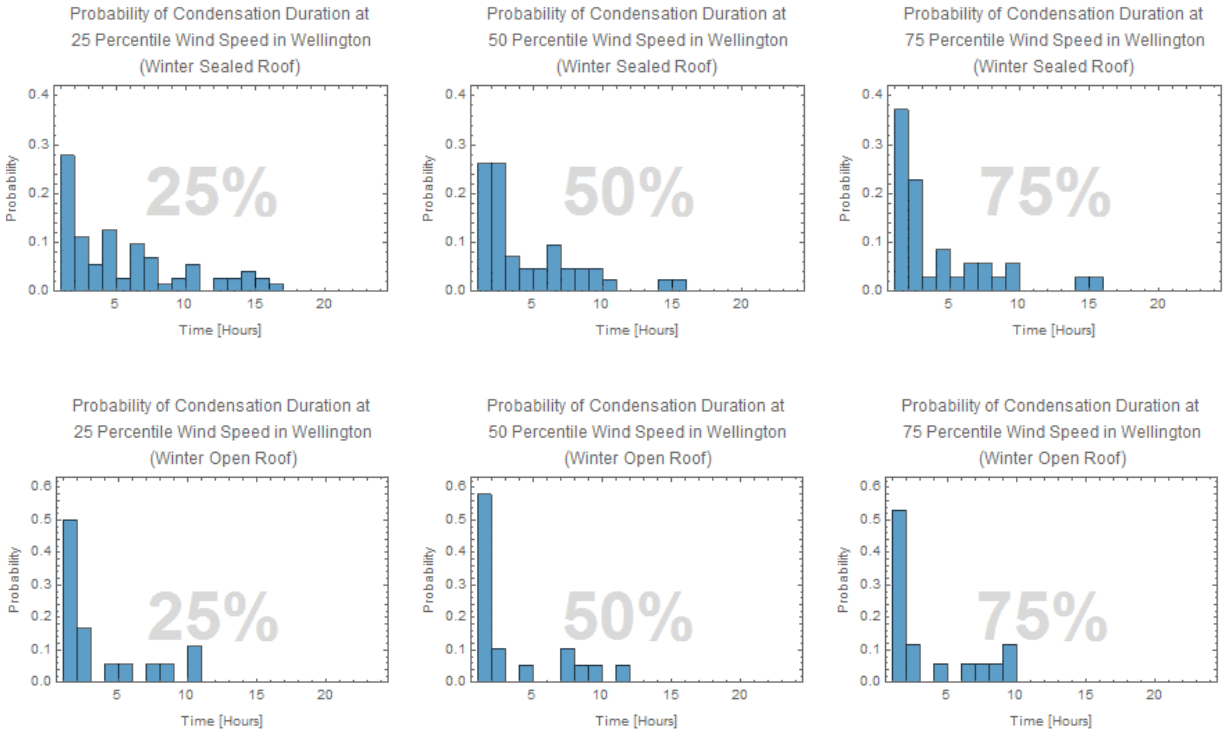

Figure 29. Condensation statistics for the gable roof in the Wellington zone for the winter months and the three wind speeds: comparison between open and closed vents.

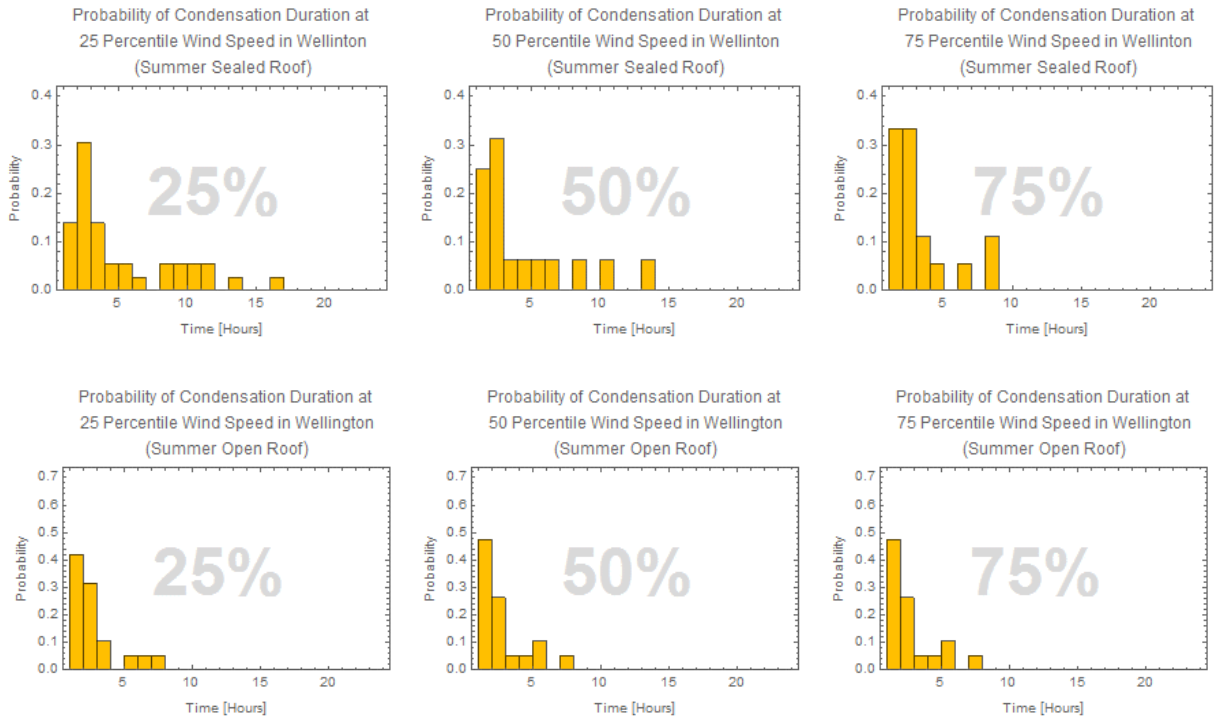

Figure 30. Condensation statistics for the gable roof in the Wellington zone for the summer months and the three wind speeds: comparison between open and closed vents.

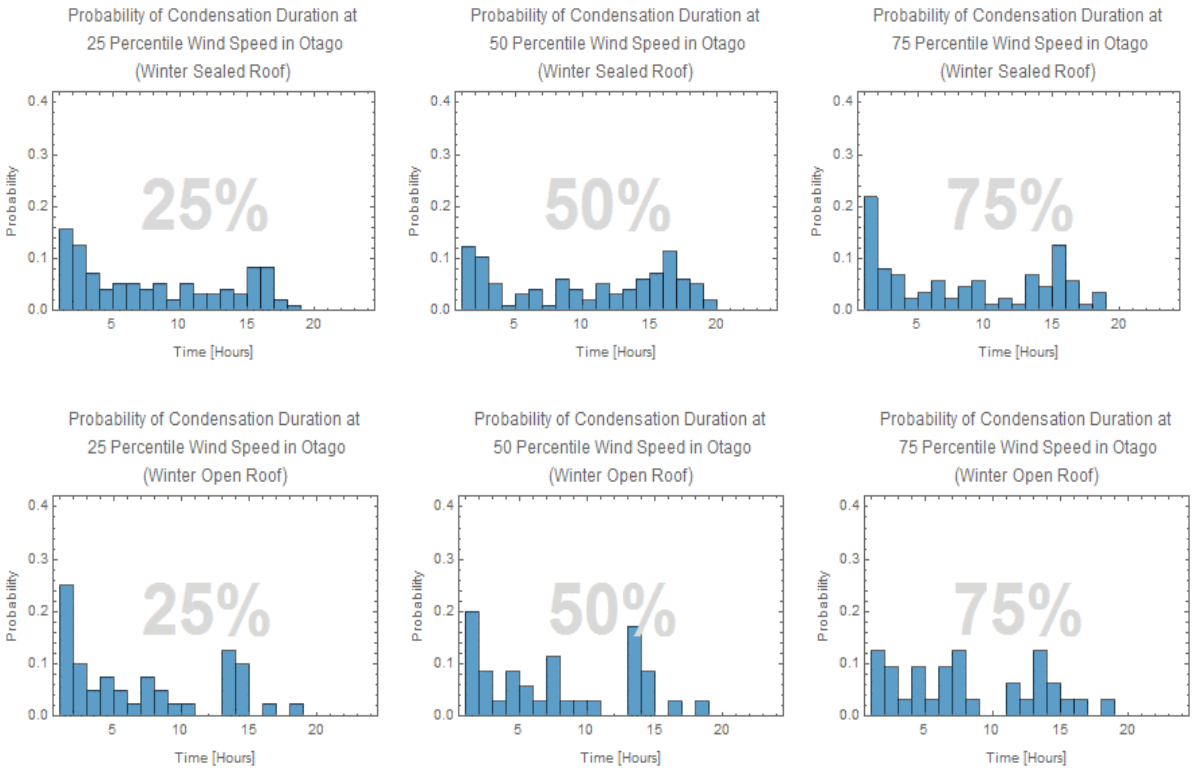

Figure 31. Condensation statistics for the gable roof in the Central Otago zone for the winter months and the three wind speeds: comparison between open and closed vents

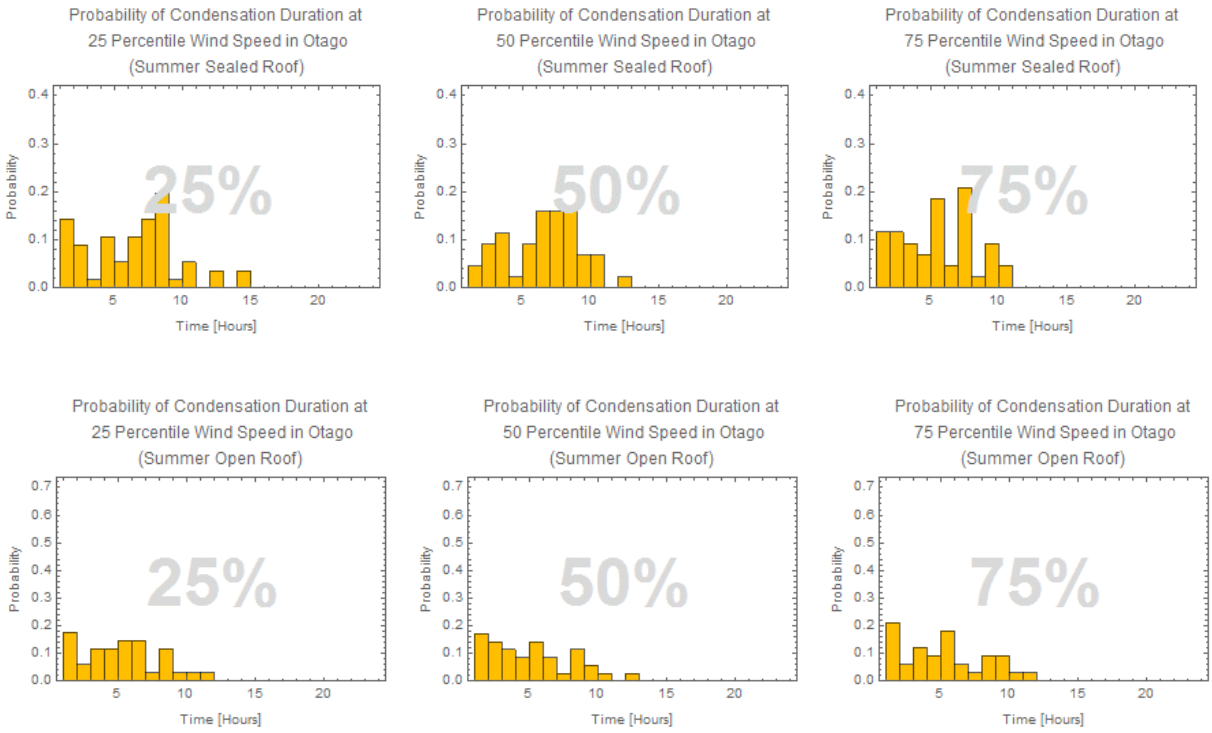

Figure 32. Condensation statistics for the gable roof in the Central Otago zone for the summer months and the three wind speeds: comparison between open and closed vents.

4.3 Skillion roof

The condensation conditions of the skillion roof are considerably worse compared to the gable roof (section 4.2). The calculations were prohibitively long due to the prolonged condensation conditions, which causes the numerical solver to conduct very small time steps. The skillion roof model was therefore run differently from the gable roof simulation. An optimal ventilation of 0.5 ACH was set in the living quarters. The roof ventilation was then varied between 14 and 66 ACH. The transport of moist air from the living quarters into the roof cavity was set to 10^{-4} m^3/m^2s. Figure 33 shows the indoor relative humidity during the winter period as used by the simulation model. The temperature of the indoor environment was set to a constant 293 Kelvin (20°C). With the given indoor and outdoor climate, the condensation probability was calculated over the 92-day winter period 1 June to 31 August for four locations in Auckland, Taupo/Turangi, Wellington and Central Otago.

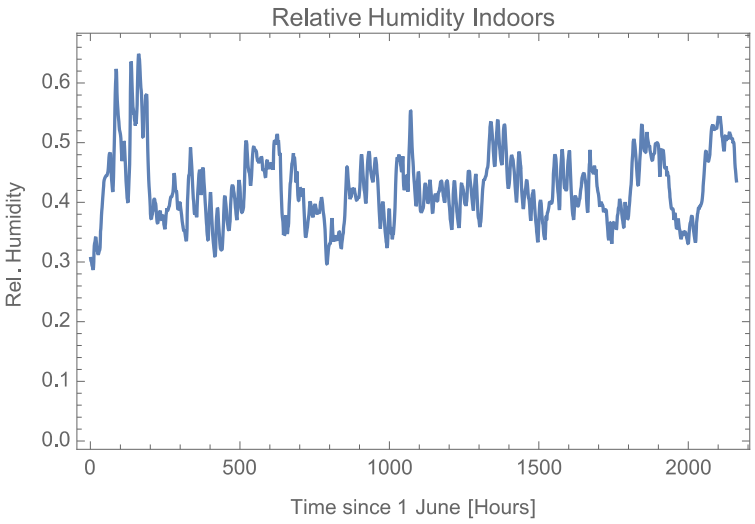

Figure 33. Indoor relative humidity during the winter period with an indoor air infiltration of about 0.5 ACH.

The results are shown in Figure 34, where the condensation probability at the four locations is plotted depending on the roof outdoor air exchange.

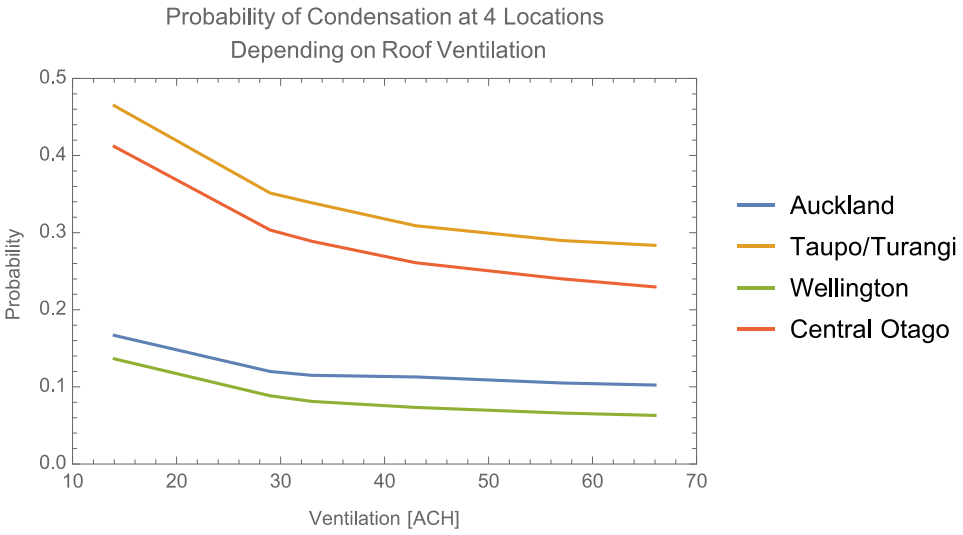

Figure 34. Condensation probability in the roof cavity depending on roof ventilation and geographic location during winter.

The drop in condensation probability is reasonably large at all four locations when increasing the air exchange from 14 to 33 ACH. Further increase in air exchange achieves only moderate improvements for Auckland and Wellington but stronger improvements for Central Otago and Taupo/Turangi.

It should be noted that the values these graphs show depend on the moisture load indoors and the air transport between indoors and the roof cavity. The source of most condensation events in the roof is the moisture originating from the room underneath the roof. Avoiding high moisture loads in the room by ventilation is therefore of importance to a performing roof and so is the amount of air that is transported through the ceiling.

There is an average pressure gradient of 4 Pa across the ceiling towards the roof cavity transporting air from the room into the roof cavity. Improving the airflow resistance of the ceiling and other structures connected to the roof will help the roof to manage moisture.

The dependence of the roof condensation probability on the room ventilation or, for that matter, room moisture load is shown in Figure 35 where the Central Otago climate was used to calculate condensation. From the graph, it is apparent that proper moisture management in the room will have a strong impact on the moisture performance of the roof. Ventilating the room to the recommended 0.4 to 0.6 ACH will drop the condensation considerably. The roof ventilation was set to about 33 ACH. The red dot in Figure 35 identifies the outdoor-indoor air exchange rate that was used in all subsequent simulations.

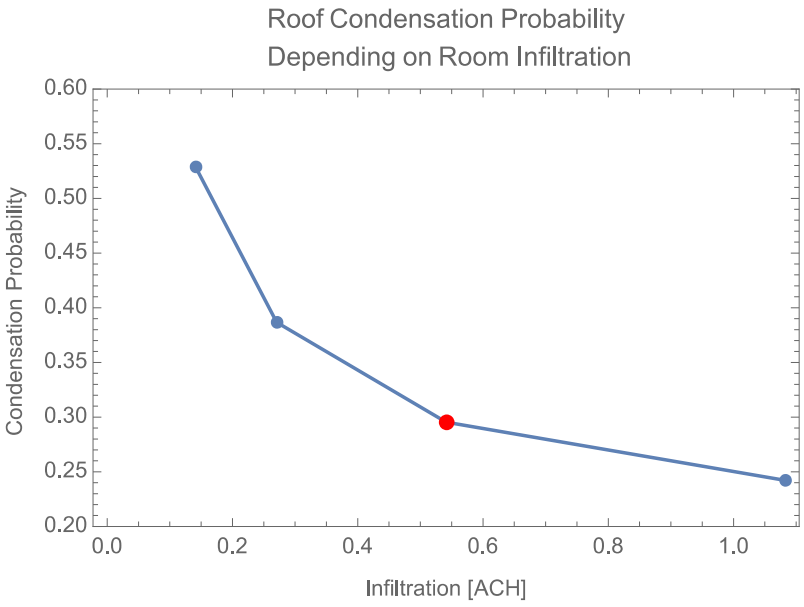

Figure 35. Example from Central Otago showing the dependence of the roof condensation probability on the indoor-outdoor room air exchange rate. The red dot is at about 0.55 ACH, which is within range of the air exchange rate recommended by the World Health Organisation. This exchange rate is then used in all subsequent simulations.

Figure 36 shows the impact of roof ventilation on roof condensation probability. The results here are based on a room ventilation of about 0.5 ACH. One can see that the ventilation of the roof cavity will improve the condensation probability further.

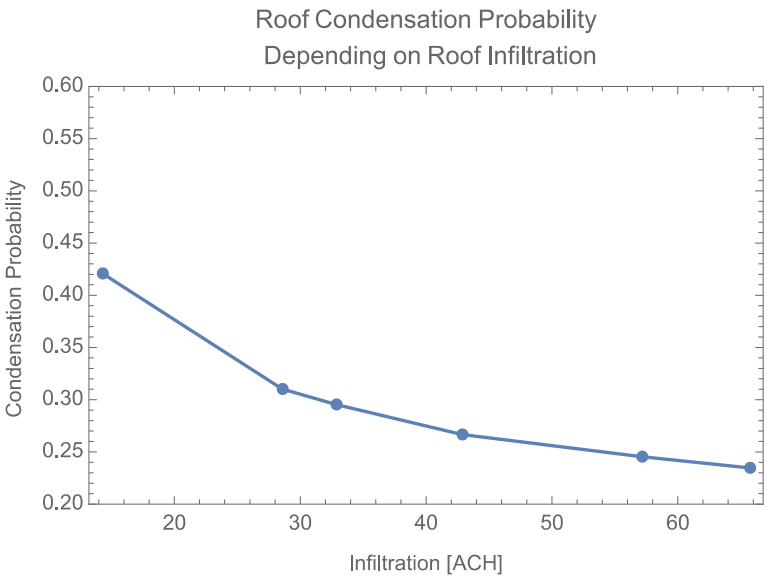

Figure 36. Impact of roof ventilation on the condensation probability. The results are based on a room ventilation of about 0.5 ACH.

Figure 37 to Figure 40 show the distribution of the condensation length at the four locations during winter at roof air exchange rates between 14 and 66 ACH. The condensation hours are predominantly shorter than 24 hours, allowing the condensate to evaporate before the next day/night cycle starts. The distributions are depending on the local climate. Auckland and, in particular, Wellington have shorter condensation events that last mostly 5 hours or less. Taupo/Turangi and Central Otago exhibit short events but also considerable probability of events lasting around 15 hours.

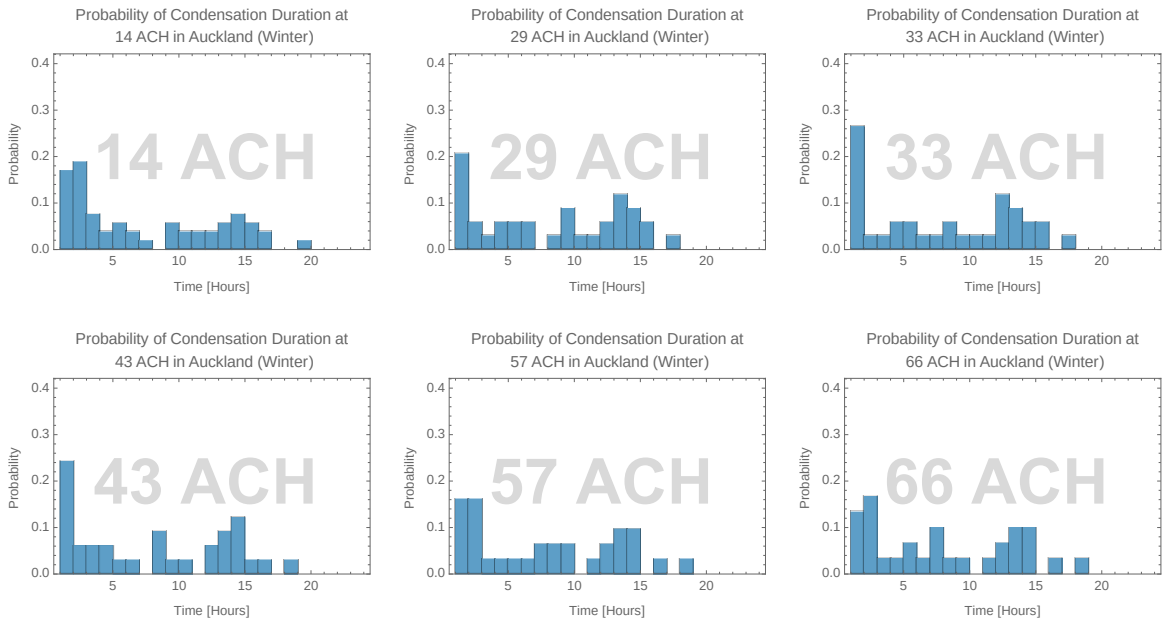

Figure 37. Condensation hour distribution for Auckland at roof air exchange rates between 14 to 66 ACH.

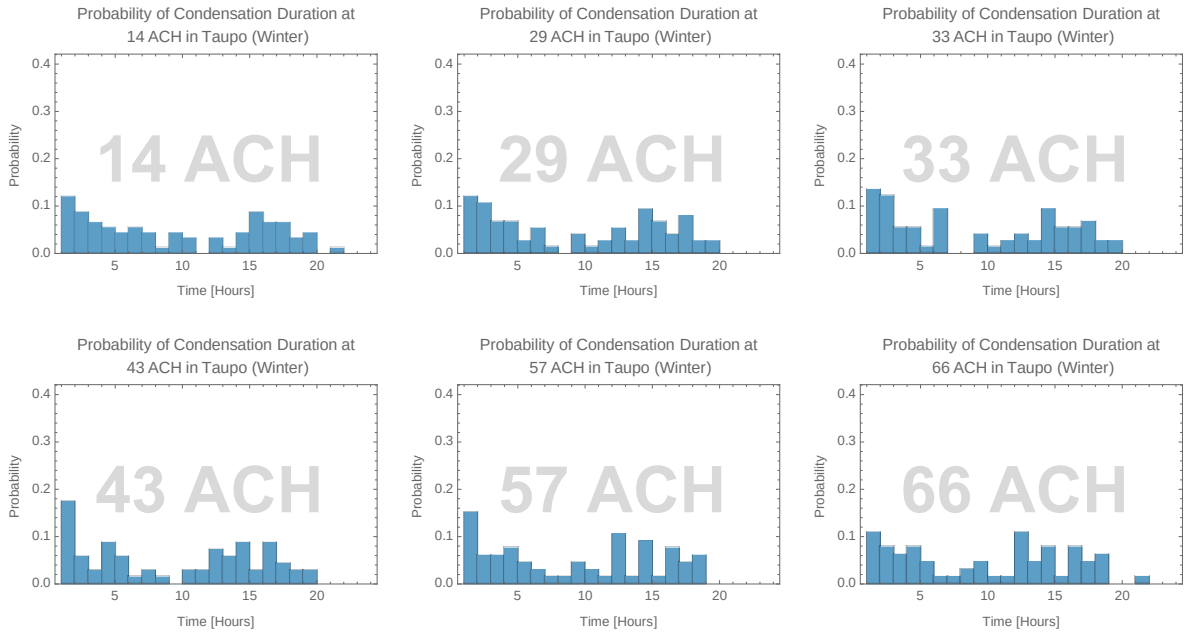

Figure 38. Condensation hour distribution for Taupo/Turangi at roof air exchange rates between 14 to 66 ACH.

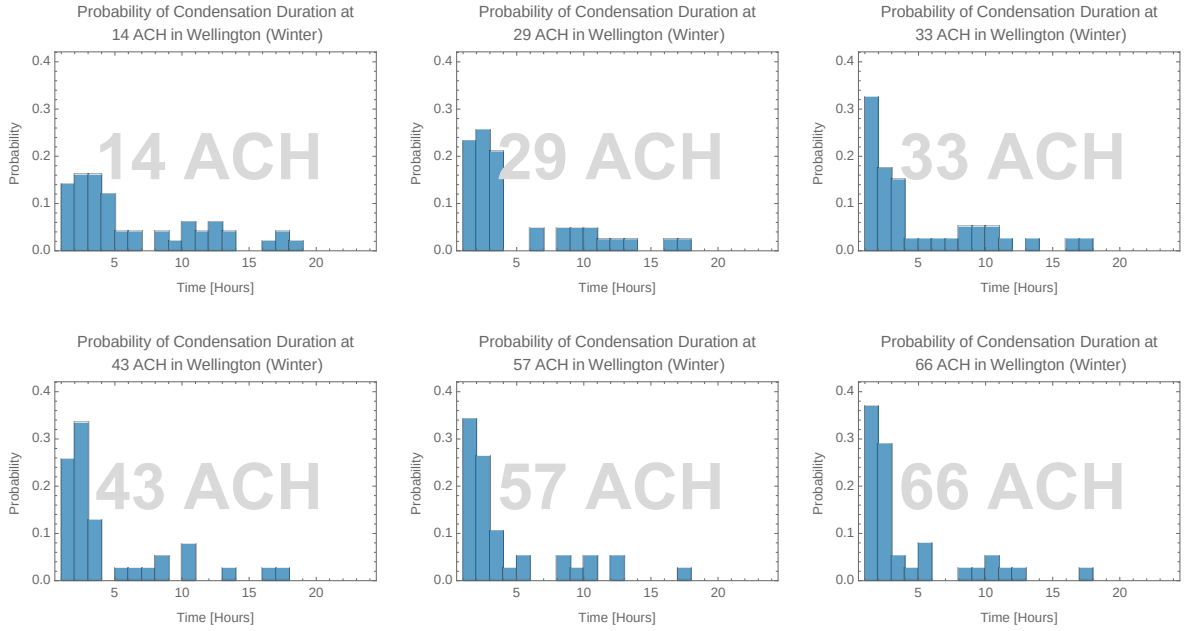

Figure 39. Condensation hour distribution for Wellington at roof air exchange rates between 14 to 66 ACH.

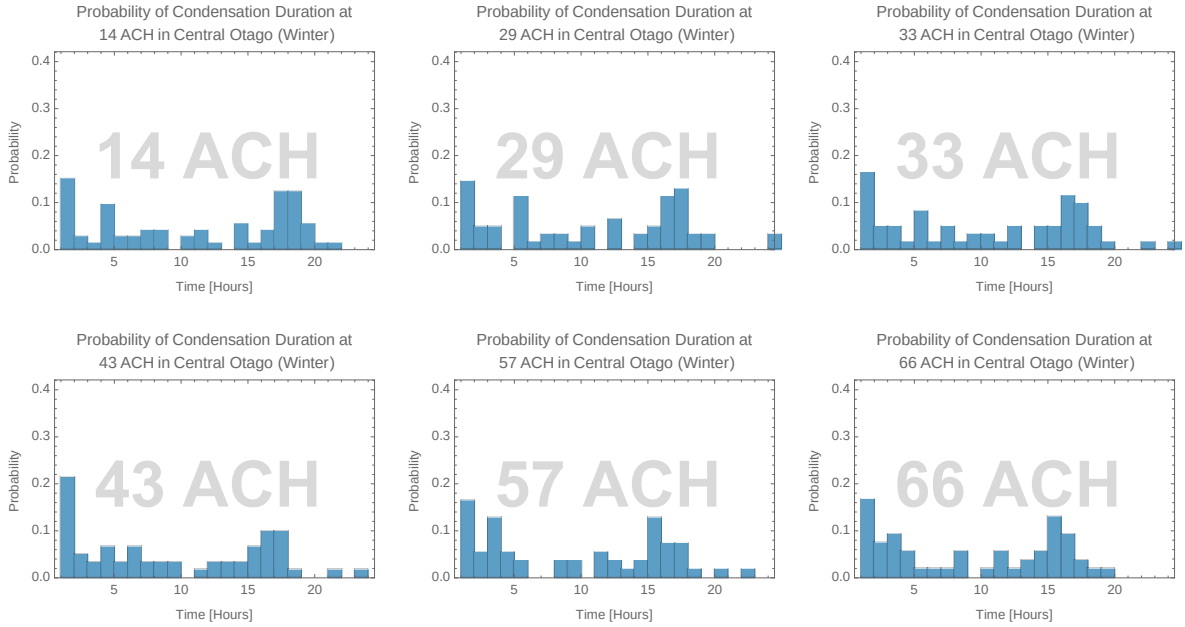

Figure 40. Condensation hour distribution for Central Otago at roof air exchange rates between 14 to 66 ACH.

Table 19 shows the percentage of time the underside of the roof cladding will have condensation conditions depending on the outdoor-roof air exchange rate.

Condensation risk is high for the locations of Taupo/Turangi and Central Otago and considerably lower for Auckland and Wellington. Noticeable is also the drop in ventilation effectiveness as the exchange rate increases. Very high exchange rates have little effect on the condensation risk.

Table 19. Percentage of time the skillion roof cladding will be under condensation condition depending on the outdoor-roof air exchange rate.

Location	14 ACH	29 ACH	33 ACH	43 ACH	57 ACH	66 ACH
Auckland	17%	12%	12%	12%	11%	10%
Taupo/Turangi	48%	36%	35%	32%	30%	29%
Wellington	14%	9%	8%	8%	7%	6%
Central Otago	42%	31%	30%	27%	25%	23%

5. Conclusion

We have used our nodal model approach to evaluate the risk of condensation events in a variety of roof cavity configurations. The tool that has been developed at BRANZ is flexible, stable and reliable enough to cope with a wide variety of complex interactions and input parameters. The input parameters to the simulation have been found to be critical. The risk of high moisture load on roof cladding is strongly dependent on the location of the building, its orientation and exposure to sun and wind, the use of the building and the indoor climate of the rooms underneath the roof, to name the most important factors.

The perfectly ventilated open steel roof described in section 4.1 shows that, during condensation conditions caused by radiative under-cooling, the outside air can become a source of moisture that condensates on the inside of the cladding. In closed roofs that are sitting above rooms with higher than outside temperature, this risk is somewhat moderated, as the warmer room raises the temperature of the roof cavity through the finite insulation by a few degrees.

The gable roof without additional ventilation openings was found to experience condensation events, especially on calm days. These condensation events were reduced by the installation of vent openings to the soffit and the ridge. While buildings in the colder climates of Taupo/Turangi and Central Otago will benefit from additional roof ventilation – for instance, from 17% without vents to 12% with vents for Taupo and average wind speeds – the benefit seems to be more significant for the Auckland region with its higher ambient moisture content. A general trend is also visible in that the installation of vents seems to reduce the length of a given condensation event.

The skillion roof simulations proved to be more difficult due to much longer calculation times caused by prolonged condensation conditions. The latter were caused by the assumption of a very airtight roof cavity in combination with a small cavity space. The consequently adopted approach to conduct the simulation based on a variation of roof cavity air exchanges proved to be more successful. Again, we find that increasing the air exchange rates in the cavity of a skillion-type roof reduces the overall risk of condensation. The benefits from increasing the ventilation rates beyond approximately 35 ACH are marginal however.

An important finding is the demonstration of roof cavity condensation risk as a function of ventilation of the living spaces of a building. Adopting the recommended ventilation rate of approximately 0.5 ACH in the main part of the building has been demonstrated to significantly reduce the number of condensation events in a skillion-type roof for instance.

This underlines to importance to occupant behaviour in modern, more airtight buildings. The generation of moisture indoors needs to be minimised, any excess moisture needs to be removed by adequate ventilation and airflows from downstairs into the roof cavity need to be minimised.

References

ASHRAE. (2005). *ASHRAE HANDBOOK Fundamentals*. American Society of Heating, Refrigerating and Air-Conditioning Engineers Inc., Atlanta. ISBN 1-931862-71-0

BRANZ. (2015). *Initial guidance on the moisture design of large-span roofs for schools*. BRANZ Discussion Document, BRANZ Ltd, Porirua. ISSN:1179-6197

Cunningham, M. (1980). Modelling of moisture transfer in structures – I. A description of finite-difference nodal model. *Building Environment,* 25, 55–61.

Cunningham, M.J. and Quaglia, L. (2013). *Remediating condensation problems in large-cavity, steel-framed institutional roofs*. Study Report SR289, BRANZ Ltd, Porirua.

Elkink, A. (2012). *Internal Moisture*. BRANZ Building Basics. BRANZ Ltd, Porirua.

Iffa, E. and F. Tariku, F. (2015). Attic baffle size and vent configuration impacts on attic ventilation. *Building and Environment,* 89, 28–37.

Kehrer, M. (2008). Radiation effects on exterior surfaces. *WUFI Workshop NBI/SINTEF 2008*. Trondheim.

Liley, J.B., Shiona, H., Sturman, J. and Wratt, D.S. (2007). *Typical Meteorological Years for the New Zealand Home Energy Rating Scheme*. NIWA, Wellington.

Rose, W.B. (1992). Measured values of temperature and sheating moisture content in residential attic assemblies. *Thermal Performance of the Exterior Envelopes of Buildings* V, 379–390.

Sherman, M.H. (1990). Tracer-gas techniques for measuring ventilation in a single zone. *Building and Environment,* 24(4), 365–374.

Trethowen, H.A. (1987). Air, earth, water - the sources of moisture. *New Zealand Workshop on Airborne Moisture Transfer*, Wellington.

Walton G. and Dols, S. 2010. *CONTAM Multizone Modeling Website*. National Institute for Standards and Technology (NIST), USA, 14 December. (Online). Available: http://www.bfrl.nist.gov/IAQanalysis/CONTAM/index.htm. (Accessed 27 August 2015).